THE JOURNAL OF PHYSICAL CHEMISTRY A
A JOURNAL OF THE AMERICAN CHEMICAL SOCIETY

pubs.acs.org/JPCA Article

Efficient, Direct Calculation of Reaction Rate Coefficients Based on a Partially Rearranged Rovibrational Hamiltonian: A Full-Dimensional Case Study of the H_2 + D → HD + H Reaction

Published as part of The Journal of Physical Chemistry A special issue "John F. Stanton Memorial Issue".

Gábor A. Ecseri, Attila G. Császár, and Csaba Fábri*

Cite This: *J. Phys. Chem. A* 2026, 130, 6312–6326 Read Online

ABSTRACT: It is shown that an efficient, "direct", and fully quantum mechanical calculation of thermal reaction rate coefficients requires a new, partially rearranged form of the numerically constructed exact kinetic energy part of the rovibrational Hamiltonian expressed in internal coordinates. Using this Hamiltonian and an accurate, full-dimensional potential energy surface characterizing the H_2 + H exchange reaction, developed by Mielke, S. L. et al. *J. Chem. Phys.* **2002**, *116*, 4142–4161, reaction rate coefficients in the temperature range of 75–800 K have been computed for the H_2 + D → HD + H reaction. The paper puts particular emphasis on the exact treatment of overall molecular rotation and on nuclear spin symmetry.

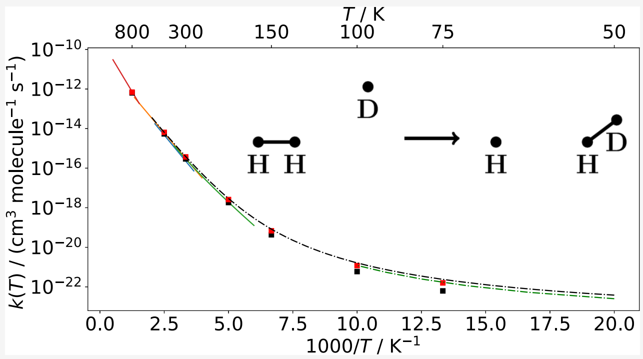

■ INTRODUCTION

During the last century, several models and algorithms have been developed that allow for the interpretation and computation of thermal reaction rate coefficients, $k(T)$, of gas-phase reactions. The most practical approaches include classical and semiclassical methods[1−4] and methods based on (variational) transition state theory.[5−12] Since there are several excellent reviews and textbooks covering these approximate models,[10−16] we are not considering them any further. Determination of state-to-state reaction probabilities through the detailed quantum mechanical study of molecular collision events can also lead to thermal reaction rate coefficients,[17,18] but for practical purposes, this is a somewhat complicated and inefficient approach if no detailed state-to-state information is needed.

It was recognized more than half a century ago[3,19] that there exists an efficient, "direct" way for the quantum-chemical computation of thermal reaction rate coefficients. This approach is especially useful for chemical reactions where there are no long-lived resonance states significantly affecting the outcome of the collision between the reaction partners.

The direct approach to the calculation of $k(T)$ quantum mechanically was developed into an efficient algorithm first by Miller et al.[3,20−24] and then by Manthe et al.[18,25−31] There are a few further notable studies based on and advancing this formalism.[32−37] The principal characteristics of this direct approach, followed in this study, are as follows: (a) it relates the reaction rate coefficient to the flux through a dividing surface that separates reactants from products; (b) the central quantity of the formalism is the thermal flux operator, which has only a relatively small number of nonvanishing eigenvalues; thus, the corresponding eigenstates can be obtained efficiently and short-time dynamics is sufficient for the converged determination of the rate; (c) no separability within the coordinates is required: there is no "reaction coordinate" separable from the rest of the coordinates; (d) no direct information is needed about the asymptotic (reactant and product) states; and (e) the dynamical information in a reactive region close to a potential barrier provides the path to the $k(T)$ coefficients without the need for a detailed solution of the state-to-state reactive scattering problem.[23,38]

There are many possible forms of the exact rovibrational Hamiltonian[39−45] appearing in the equations of the direct method; in theory, all of them are equivalent. It is important to emphasize that the Eckart–Watson[40,41,44,45] form, which is also exact, cannot be considered in applications where the atoms rearrange. Forms of the Hamiltonian expressed in

Received: February 27, 2026
Revised: April 28, 2026
Accepted: July 6, 2026
Published: July 28, 2026

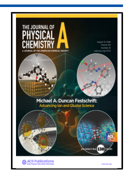

https://doi.org/10.1021/acs.jpca.6c01349
J. Phys. Chem. A 2026, 130, 6312–6326

internal coordinates should almost always be appropriate. Nevertheless, one must be aware that, in different applications, different forms of the Hamiltonian may perform differently[42,46] as their use may result in different numerical issues. It has remained unclear what the best form of the rovibrational Hamiltonian is for thermal reaction rate computations.

Despite its formal appeal, practical computations using the formalism developed by Miller, Manthe, and their co-workers remain somewhat limited. Probably the most important reasons are as follows: (a) other ways to compute $k(T)$ are significantly less demanding computationally when quantum effects are not overwhelmingly important; (b) general-purpose, black-box-type codes that could be used for cases involving more than four atoms have not yet been developed; and (c) the exact inclusion of overall rotational motion seems particularly cumbersome and expensive. The present paper addresses the latter two points.

The exact inclusion of overall rotation in direct thermal reaction rate coefficient calculations can be challenging, even for the H_3 system.[47] The following are the most typical approximations used for the inclusion of rotational excitation in the calculation of reaction rate coefficients: (a) in the J-shifting (angular momentum shifting) approach,[48−51] reaction probabilities at nonzero total angular momentum ($J > 0$) are related to those at $J = 0$ through a shift in the rotational energy (and consequently the rotational partition function); and (b) during the centrifugal sudden (coupled states) approximation,[52,53] the rotational−vibrational coupling term, also called the Coriolis term, is completely neglected. Testing the limitations of these models (and their generalizations) for various systems (see, *e.g.*, refs 50, 51, 54, and 55) is an interesting topic in itself.

We decided to test the "direct" approach followed during this study on perhaps the most thoroughly studied chemical reaction, the gas-phase exchange reaction of H_2 + H,[56−58] by applying the method to the isotopic variant H_2 + D → HD + H. There are several reasons for this choice: (a) studying isotopic variants of the prototypical gas-phase H_2 + H exchange reaction has a rich history,[5,56,57,59−63] with particularly strong participation, especially in the early years, from scientists born in Hungary; (b) knowledge of a single potential energy surface (PES) appears to be sufficient, as first pointed out in a ground-breaking paper by London,[64] for the accurate computation of its thermal reaction rate coefficients; (c) there is a significant number of experimental results available,[65−84] including ones that showed a curvature in the Arrhenius plot for the H_2 + D reaction at low temperatures;[69,72] (d) isotopic variants of the H_2 + H reaction have been subjected to computational studies of varying sophistication,[5,69,85−107] some indicating that, using less accurate PESs, there are deviations between the experimental and the computational reaction-rate studies, both at low (200 K) and high (1500 K) temperatures; and (e) at the transition state, both the vibrational and the rotational wavenumbers are relatively large, facilitating the convergence of the "direct" modeling approach.

Computing thermal reaction rates requires a PES. Over the last 60 years, several full-dimensional PESs have been computed for the three-electron H_3 system[108−118] (for a historical overview of the earlier PESs see refs 57 and 117). These PESs include, in alphabetical order, the BKMP,[114] BKMP2,[115] CCI,[117] DMBE,[113] EQMC,[116] LEPS,[112] and LSTH[108−111] variants. In this paper, results are reported only for the CCI PES of ref 117. Within the standard Born−Oppenheimer[119] approximation, these PESs are independent of the masses and nuclear spins. Corrections due to the diagonal Born-Oppenheimer correction (DBOC)[120,121] were also reported,[117] they have particular relevance for the lightest molecular systems. Note that a significant number of dynamical results (cross sections, reaction rate constants, and resonances) from statistical, reduced-dimensionality, semiclassical, and full quantal studies have been presented using the BKMP, BKMP2, CCI, DMBE, and LSTH surfaces.[87,95−97,99,100,103,122−131]

Experimental measurements of the thermal reaction rate coefficients of the H_2 + D → HD + H reaction are available over a temperature range of 167−2112 K.[66,67,69,71,73−79,82−84,129,132] Considering the variety of experimental techniques used to produce $k(T)$ values, most of them agree reasonably well. Particularly useful experimental data[82,83] have been provided by the flash photolysis−shock tube technique. The experimental data have provided a fertile and stringent testing ground for the computational studies.

Finally, the hallmarks of the present computational study: (a) it takes advantage of a fully numerical approach offered by the general, black-box type GENIUSH algorithm and code,[42,43] allowing the straightforward use of arbitrary internal coordinates, body-fixed frame embeddings, and reduced-dimensional models for exploring the power of the "direct" method to compute thermal reaction rate coefficients; (b) it uses a new form of the exact kinetic energy operator, called the partially rearranged form, which is needed to obtain correct reaction rate coefficients; (c) it includes the rotational and nuclear spin degrees of freedom in the numerically exact computations, which are crucial for thermal reaction rate computations; and (d) it yields results that are in good agreement with earlier experimental and computational studies for the H_2 + D → HD + H reaction.

■ METHODOLOGY

The "Direct" Method

As foreseen by Yamamoto[19] and elaborated by Miller et al.,[20] thermal reaction rate coefficients of bimolecular reactions at temperature T can be obtained from the standard flux autocorrelation function $C_f^T(t)$ as a time (t) integral:

$$k(T) = \frac{1}{Q_r(T)} \int_0^\infty C_f^T(t) \mathrm{d}t \tag{1}$$

where $Q_r(T)$ is the partition function of the reactants (per unit volume). In a quantum mechanical context, the standard time-dependent flux autocorrelation function of eq 1 can be expressed as

$$C_f^T(t) = \mathrm{Tr}[e^{-(\beta\hat{H})/2}\hat{F}e^{-(\beta\hat{H})/2}e^{\mathrm{i}\hat{H}t/\hbar}\hat{F}e^{-\mathrm{i}\hat{H}t/\hbar}] \tag{2}$$

where $\hat{H}$ is the (rovibrational) Hamiltonian of the system, $\hat{F}$ is the reactive flux operator, $\hbar$ is the reduced Planck constant, and $\beta = 1/(kT)$, where k is the Boltzmann constant and T is the thermodynamic temperature. The reactive flux operator is defined as $\hat{F} \coloneqq \mathrm{i}/\hbar[\hat{H}, \theta(s(\mathbf{q}))]$ where $\theta(x) = \begin{cases} 0, & x < 0 \\ 1, & x \geq 0 \end{cases}$ is the Heaviside step function. The reactant and product configurations are separated by a dividing surface, $s(\mathbf{q}) = 0$. The multivariate function $s(\mathbf{q})$, dependent on the internal

https://doi.org/10.1021/acs.jpca.6c01349
J. Phys. Chem. A 2026, 130, 6312−6326

coordinates $\mathbf{q}$ chosen for the system, has negative/positive values for the reactant/product configurations.

The quantum mechanical trace in eq 2 should be evaluated using a suitable basis; in the present work, we utilize a methodology in which the trace is evaluated in the eigenbasis of the so-called thermal flux operator.[18,133] The thermal (sometimes called Boltzmannized[133,134]) flux operator is defined as

$$\hat{F}(\beta) := e^{-(\beta\hat{H})/2}\hat{F}e^{-(\beta\hat{H})/2} \tag{3}$$

Then, eq 2 can be rewritten as

$$C_f^T(t) = \sum_i f_i \langle\phi_i(t)|\hat{F}|\phi_i(t)\rangle \tag{4}$$

where $\hat{F}(\beta)\,|\phi_i\rangle = f_i\,|\phi_i\rangle$ and $|\phi_i(t)\rangle = e^{-\mathrm{i}\hat{H}t/\hbar}\,|\phi_i\rangle$. As pointed out before, see, e.g., ref 134, $\hat{F}(\beta)$ is a low-rank operator, and its eigenvectors corresponding to the largest (in absolute value) eigenvalues provide a compact basis to evaluate the operator trace in eq 2 and obtain a converged value based on just a relatively small number of eigenstates.

Once the thermal flux eigenpairs are obtained at a single temperature, T, the standard flux autocorrelation function at $T/2$ can also be computed straightforwardly as[24]

$$C_f^{T/2}(t) = \sum_{ij} f_i f_j \left|\langle\phi_j|\phi_i(t)\rangle\right|^2 \tag{5}$$

Since $\langle\phi_j|e^{-\mathrm{i}\hat{H}t/\hbar}\phi_i\rangle = \langle(e^{-\mathrm{i}\hat{H}t/(2\hbar)}\phi_j^*)^*|e^{-\mathrm{i}\hat{H}t/(2\hbar)}\phi_i\rangle$, by propagating the thermal flux eigenvectors up to $t/2$, $C_f^{T/2}$ can be obtained at time t.[26] Note that in the literature, several other, more complicated techniques have been described that can be used to compute reaction rate coefficients at several different temperatures from a single diagonalization of the thermal flux at a chosen reference temperature.[25,26,35]

Since the thermal flux operator commutes with the overall angular momentum operator $\hat{J}$, the thermal flux can be diagonalized for each rotational quantum number J separately; that is, $\hat{F}^J(\beta)|\phi_i^J\rangle = f_i^J|\phi_i^J\rangle$. Thus, separate flux autocorrelation functions $C_f^{T,J}(t)$ and reaction rate coefficients $k^J(T)$ can be computed. The full thermal reaction rate coefficient is a simple sum of these:

$$k(T) = \sum_J (2J+1)k^J(T) \tag{6}$$

If indistinguishable atoms are present in the reactive system, we must take the Pauli exclusion principle into consideration. Thus, in the computation of the reaction rate coefficient, the basis used to evaluate the trace of eq 2 must be symmetric or antisymmetric with respect to the exchange of identical bosons or fermions, respectively. In the present application, the basis consists of the product of thermal flux eigenstates and nuclear spin states. Earlier, nuclear spin states were not mentioned, as the operators within the trace of eq 2 do not act on the spin coordinates. However, it is now necessary to include the nuclear spin states of the system, since they become relevant when the Pauli exclusion principle is taken into account.

The effects caused by the involvement of identical atoms in a reaction, that is, the consideration of nuclear spin states, should be considered for all collisions and binary reactions.[135,136] For example, in the case of H_2 in the H_2 + D → HD + H reaction, there are three symmetric (*ortho*, $I = 1$, where I denotes the nuclear spin quantum number) nuclear spin state functions: $(1/\sqrt{2})(\alpha(1)\beta(2) + \alpha(2)\beta(1))$, $\alpha(1)\alpha(2)$, and $\beta(1)\beta(2)$ and there is one antisymmetric (*para*, $I = 0$) nuclear spin state function, $(1/\sqrt{2})(\alpha(1)\beta(2) - \alpha(2)\beta(1))$. $\beta(1)/\alpha(1)$ denotes that $H^{(1)}$ is in β/α nuclear spin states, respectively, and similarly for $H^{(2)}$. The thermal flux eigenstates have a well-defined symmetry property only if the thermal flux operator commutes with all the permutation operators of the equivalent atoms, $\hat{P}_{ij}$. The commutator of $\hat{P}_{ij}$ and the thermal flux can be expressed as

$$\begin{aligned}[\hat{P}_{ij}, \hat{F}(\beta)] &= e^{-(\beta\hat{H})/2}[\hat{P}_{ij}, \hat{F}]e^{-(\beta\hat{H})/2} \\ &= \frac{\mathrm{i}}{\hbar}e^{-(\beta\hat{H})/2}[\hat{H}, [\hat{P}_{ij}, \theta(s(\mathbf{q}))]]e^{-(\beta\hat{H})/2}\end{aligned} \tag{7}$$

Here, we have exploited the fact that $[\hat{P}_{ij}, \hat{H}] = 0$. Therefore, if the dividing surface is chosen so that $[\hat{P}_{ij}, \theta(s(\mathbf{q}))] = 0$, $\hat{P}_{ij}$ commutes with the thermal flux.

In the case of the H_2 + D → HD + H reaction, it is possible to guarantee that $[\hat{P}_{12}, \theta(s(\mathbf{q}))] = 0$. Therefore, thermal flux eigenstates are either symmetric or antisymmetric under the exchange of $H^{(1)}$ and $H^{(2)}$ ($\hat{P}_{12}$). To enforce the Pauli exclusion principle, symmetric/antisymmetric thermal flux eigenstates must be paired with antisymmetric/symmetric (*para*/*ortho*) nuclear spin states of the two protons. This is the basis used in this study to evaluate the trace of eq 2, which can be carried out separately using only the *ortho* or only the *para* states, resulting in the $C_f^{\mathrm{ortho}}(t)$ or $C_f^{\mathrm{para}}(t)$ flux autocorrelation functions, respectively, and finally in the $k^{\mathrm{ortho}}(T)$ or $k^{\mathrm{para}}(T)$ reaction rate coefficients. Since the operators within the trace are independent of the nuclear spin, the three $k^{\mathrm{ortho}}(T)$ contributions are equal, yielding a spin statistical factor of $g = 3$. Generally, the full thermal reaction rate coefficient can be written as the sum of the contributions from the different nuclear spin states,

$$k(T) = \sum_i g_i k^i(T) \tag{8}$$

and in the specific case of the H_2 + D → HD + H reaction,

$$k(T) = 3k^{\mathrm{ortho}}(T) + k^{\mathrm{para}}(T) \tag{9}$$

■ GENIUSH

The set of codes GENIUSH,[42,43,137−143] upon which the present study is based, is a general, black-box type, completely numerical quantum-chemical code designed[42,43] to solve the time-independent nuclear Schrödinger equation for rovibrational energy levels and eigenstates in a (quasi-)variational fashion. GENIUSH uses the exact and general kinetic energy operator constructed numerically; therefore, no analytical form of the kinetic energy is needed. GENIUSH can accommodate any set of internal coordinates, any embedding of the molecular (body-fixed) axes, and can solve arbitrary, reduced- or full-dimensional molecular models.

In GENIUSH, the matrix representation of the rovibrational Hamiltonian is set up in a multidimensional direct-product discrete-variable representation (DVR)[144] basis. Since every coordinate-dependent operator $f(\mathbf{q})$ has a diagonal matrix representation in DVR and the diagonal entries are simply the values of $f(\mathbf{q})$ at the DVR points, the numerical treatment of the potential energy surface and the dividing surface is greatly simplified. Due to these characteristics, GENIUSH provides

https://doi.org/10.1021/acs.jpca.6c01349
J. Phys. Chem. A 2026, 130, 6312−6326

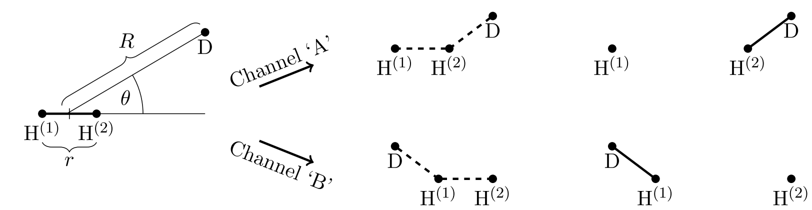

Figure 1. Schematic representation of the dividing surface as well as the reactant and product configurations of the H_2 + D → HD + H reaction. The definition of the Jacobi coordinates r, R, and θ is also displayed. Channel "A" describes the reaction in which HD is formed with $H^{(2)}$, while the reaction resulting in $H^{(1)}D$ corresponds to channel "B". The two channels are physically indistinguishable.

an ideal starting point for the development of a general code aimed at the computation of reaction rate coefficients.

The most time-consuming step of a GENIUSH computation is the determination of a given set of energy levels and eigenstates of the rovibrational Hamiltonian. In GENIUSH, the sparse DVR Hamiltonian matrix is diagonalized by the iterative Lanczos algorithm,[145,146] which requires the evaluation of matrix-vector products. While the "direct" determination of reaction rate coefficients does not require the eigenpairs of the rovibrational Hamiltonian, it does need those of the thermal flux, and the sparse DVR representation of the Hamiltonian can be employed for the representation of the thermal flux.

The Partially Rearranged Form of the Kinetic Energy Operator

It is the so-called Podolsky form[39] of the exact kinetic energy operator that has usually been used in large-scale computations of bound rovibrational quantum states performed with GENIUSH. To obtain correct reaction rate coefficients, it has become necessary to rearrange the Podolsky form of the rovibrational kinetic energy operator. The numerical issues experienced with the Podolsky form of the Hamiltonian and the solutions to them are outlined in the Appendix. The new form corresponds to a rearrangement of the vibrational kinetic energy term $\hat{T}^{\mathrm{vib}}$ in the Podolsky form, while the rotational and rovibrational coupling kinetic energy terms ($\hat{T}^{\mathrm{rot}}$ and $\hat{T}^{\mathrm{rotvib}}$, see eqs 19 and 20 of ref 43, respectively) remain unchanged.

The Podolsky form of the vibrational kinetic energy operator $\hat{T}^{\mathrm{vib}}$ in a set of internal coordinates q_k is

$$\hat{T}^{\mathrm{vib}} = \frac{1}{2}\sum_{k,l=1}^{D} \tilde{g}^{-1/4}\hat{p}_k^{\dagger} G_{kl}\tilde{g}^{1/2}\hat{p}_l\tilde{g}^{-1/4} \tag{10}$$

where the momentum operator is defined as $\hat{p}_k := -i\hbar\partial/\partial q_k$ (see ref 43 for the definition of the quantities G_{kl} and $\tilde{g}$). One can divide the double sum in eq 10 into two terms, one with $k = l$ and one where $k \neq l$:

$$\begin{aligned}\hat{T}^{\mathrm{vib}} &= -\frac{\hbar^2}{2}\tilde{g}^{-1/4}\left[\sum_{k=1}^{D}\frac{\partial}{\partial q_k}G_{kk}\tilde{g}^{1/2}\frac{\partial}{\partial q_k} + \sum_{k\neq l}^{D}\frac{\partial}{\partial q_k}G_{kl}\tilde{g}^{1/2}\frac{\partial}{\partial q_l}\right]\tilde{g}^{-1/4}\\ &= -\frac{\hbar^2}{2}\tilde{g}^{-1/4}\left[\sum_{k=1}^{D}\left(\frac{\partial(G_{kk}\tilde{g}^{1/2})}{\partial q_k}\frac{\partial}{\partial q_k} + G_{kk}\tilde{g}^{1/2}\frac{\partial^2}{\partial q_k^2}\right)\right.\\ &\quad\left. + \sum_{k\neq l}^{D}\frac{\partial}{\partial q_k}G_{kl}\tilde{g}^{1/2}\frac{\partial}{\partial q_l}\right]\tilde{g}^{-1/4}\end{aligned} \tag{11}$$

During the second step in eq 11, the first $\partial/\partial q_k$ derivative is evaluated using the product rule, acting on both $G_{kk}\tilde{g}^{1/2}$ and the subsequent derivatives. The second line of eq 11 is referred to as the partially rearranged form used to compute reaction rate coefficients in this study. Considerations regarding the hermiticity of the matrix representation of the partially rearranged form are described in the Appendix. In summary, the partially rearranged form of the kinetic energy operator is similar to the well-known Podolsky form; only the diagonal terms ($k = l$) are rearranged in $\hat{T}^{\mathrm{vib}}$.

The Thermal Flux Operator

The thermal flux operator $\hat{F}(\beta)$, see eq 3, is purely imaginary and Hermitian; thus, it has eigenvalue pairs of opposite signs and equal absolute values, along with eigenfunctions that are complex conjugates of one another. As detailed in ref 147, for example, each pair can be considered to correspond to a rovibrational state of the activated complex. The numerical treatment and diagonalization of the thermal flux operator, a step required in the algorithm used, can be accelerated by tricks similar to those employed during the development of the GENIUSH code.[42,43]

If an iterative eigensolver is used to obtain the eigenvalues and eigenvectors of the thermal flux, matrix-vector products need to be evaluated. The product of the matrix representation of the thermal flux, $\mathbf{F}(\beta)$, with a vector, $\mathbf{v}$, is carried out in three steps,

$$\mathbf{F}(\beta)\mathbf{v} = e^{-(\beta\mathbf{H})/2}(\mathbf{F}(e^{-(\beta\mathbf{H})/2}\mathbf{v})) \tag{12}$$

where $\mathbf{H}$ and $\mathbf{F}$ are the DVR matrix representations of the Hamiltonian and the flux operator, respectively. The first and last steps are multiplications by the matrix representation of the Boltzmann operator, which can be regarded as time propagation in imaginary time. Therefore, common time propagation techniques can be used. In this work, we use the so-called Chebyshev expansion of the propagator.[148−150] In principle, other propagation methods could also be used, such as the split-operator technique. However, we employed the Chebyshev propagation, as its implementation in GENIUSH is straightforward. Since the Chebyshev propagation requires only the evaluation of matrix-vector products $\mathbf{Hv}$, it is not necessary to explicitly construct and store the Hamiltonian matrix, which can become prohibitively large. The second step is the multiplication by the matrix of the reactive flux. It is performed according to

$$\mathbf{Fv} = \frac{i}{\hbar}(\mathbf{H}\boldsymbol{\theta}\mathbf{v} - \boldsymbol{\theta}\mathbf{H}\mathbf{v}) \tag{13}$$

where $\boldsymbol{\theta}$ is the diagonal matrix of $\theta(s(\mathbf{q}))$ evaluated in the multidimensional direct-product DVR basis used to represent the Hamiltonian. In total, one action of the thermal flux needs $2N + 2$ actions of the Hamiltonian, where N is the number of

https://doi.org/10.1021/acs.jpca.6c01349
J. Phys. Chem. A 2026, 130, 6312−6326

terms needed in the Chebyshev expansion, typically not exceeding a few hundred.

The ARPACK package[151] was used to perform the diagonalization of the thermal flux matrix. ARPACK is a Fortran library that uses the Arnoldi method to iteratively diagonalize complex matrices. Thermal flux eigenstates corresponding to the dominant (largest in absolute value) eigenvalues of $\mathbf{F}(\beta)$ were then propagated in time using the Chebyshev expansion method, and the flux autocorrelation function was evaluated by eq 4 for an appropriately chosen time interval.

■ COMPUTATIONAL DETAILS

This study utilizes Jacobi (also called scattering) coordinates,[152] shown in Figure 1. They are defined as follows: r is the distance between the two hydrogen atoms, R is the distance between the deuterium and the center of mass (COM) of $H^{(1)}$ and $H^{(2)}$, while θ is the angle formed by the three points $\mathbf{r}_2$, $\mathbf{r}_{COM(1,2)}$, and $\mathbf{r}_D$, where $\mathbf{r}_2$ and $\mathbf{r}_D$ are the positions of $H^{(2)}$ and D, respectively, and $\mathbf{r}_{COM(1,2)}$ is the position of the center of mass of $H^{(1)}$ and $H^{(2)}$. Figure 1 also shows the schematic representation of the two reaction channels. The body-fixed frame is defined by directing the first Jacobi vector $(\mathbf{r}_2 - \mathbf{r}_1)$ along the positive z axis and placing the second Jacobi vector $(\mathbf{r}_D - \mathbf{r}_{COM(1,2)})$ in the xz plane (with $x \geq 0$). Under the permutation of the two equivalent hydrogen atoms, the Jacobi coordinates transform as $(r, R, \theta) \xrightarrow{\hat{P}_{12}} (r, R, \pi - \theta)$ and a 180° rotation about the body-fixed x axis is needed to restore the definition of the body-fixed frame.

The dividing surface of the H_2 + D → HD + H reaction is defined such that either the distance between $H^{(2)}$ and D, or $H^{(1)}$ and D, is equal to the distance between the two hydrogen atoms. All configurations where the $H^{(2)}$-D or the $H^{(1)}$-D distance is smaller than the $H^{(2)}$-$H^{(1)}$ distance are considered products. All the other configurations are classified as reactants. Most importantly, this dividing surface is invariant to the permutation of the two hydrogen atoms ($\hat{P}_{12}$); thus, eigenfunctions of the thermal flux operator are either symmetric or antisymmetric with respect to $\hat{P}_{12}$. The symmetry properties of the thermal flux eigenfunctions under $\hat{P}_{12}$ were determined numerically by examining the eigenvectors of the thermal flux matrix $\mathbf{F}(\beta)$.

For the computation of thermal reaction rate coefficients, we have used the CCI PES developed by Mielke, Garrett, and Peterson.[117] A potential cutoff of 20,000 cm^{-1} was applied to regularize the highest eigenvalue of the Hamiltonian, as this makes the Chebyshev expansion[148−150] employed in this study more efficient. In all computations, atomic masses m_H = 1.007 825 u and m_D = 2.014 102 u have been employed.

Sine-DVR bases[153] were used along the r and R Jacobi coordinates (Figure 1). The number of basis functions and the upper limit of the grid were varied for the different computations, while the lower limits of the grid were set to 0.10 and 0.75 Å for the r and R coordinates, respectively. Legendre-DVR basis functions were used along the θ coordinate, with DVR points distributed in the range [0°, 180°]. With these grid settings, both reaction channels shown in Figure 1 are incorporated into our computations. The grid sizes and the upper limits of the grid along the r and R coordinates for the different computations can be found in Table 1. For the rotational degrees of freedom, Wang combinations of symmetric top eigenfunctions were employed.[43] Table 1 also contains the upper time integration limit used to integrate the flux autocorrelation function. With these settings, we have found that the flux autocorrelation function remains zero for a sufficiently long time before unphysical reflections from the edges of the grid set in. Therefore, choosing an appropriate upper time integration limit posed no difficulty, and no complex absorbing potential (CAP)[154] was applied during the present work.

Table 1. Selected Parameters of the Reaction-Rate Computations[a]

T/K	J_{max}	int. time limit/a.u.	grid size r	grid size R	grid size θ	upper r/R limit/Å
100	8	1900	30	30	30	3.2
150/75	8	1000/2500	36	36	30	3.6
200/100	9	1000/1900	30	30	30	3.2
300	12	1000	20	20	30	2.5
800/400	20 (12)	800	30	30	30	2.5

[a]In the case of T = 800/400 K, computations were performed for J = 0,..., 12, 20 and values of $k^J(T)$ were then obtained *via* interpolation between J = 12 and 20. "int. time limit" is the upper integration time limit used to integrate the flux autocorrelation function $C_f^T(t)$.

The determination of thermal reaction rate coefficients requires accurate reactant partition functions, $Q_r(T)$, which can be readily evaluated by the direct summation technique. Accurate ideal-gas partition functions are available for a large number of molecular systems; see, e.g., refs 155 and 156. For the H_2 molecule, refs 155 and 157 provide particularly accurate thermochemical data. The partition function of the reactants in the H_2 + D → HD + H reaction can be expressed as

$$Q_r(T) = Q_r^{transl}(T) Q_r^{int}(T) = \left(\frac{\mu}{2\pi\hbar^2\beta}\right)^{3/2} Q_r^{int}(T) \quad (14)$$

where μ is the reduced mass of H_2 and D. For this study, the internal partition function $Q_r^{int}(T)$ of H_2 was taken from ref 155.

The computations of the thermal rate coefficients were performed at T = 100, 150, 200, 300, and 800 K for all J values up to J_{max} (see Table 1 for which J_{max} value was chosen for a given temperature). The effects of rotation and nuclear spin were taken into account using eqs 6 and 9, respectively. Thermal reaction rate coefficients were also obtained at T = 75, 100, and 400 K *via* the use of eq 5. Thus, the reaction rate coefficient at 100 K was computed by two different methods, enabling a check of the performance of eq 5.

Despite the fact that optimization of the code has not been our major focus, for J = 0, the calculation time is trivial for the H_2 + D → HD + H reaction; it takes only a few minutes of CPU time. The two most expensive parts of the reaction rate calculations are the Arnoldi diagonalization and the time evolution; the diagonalization typically takes about 10−20% of the total CPU time (slightly more for the lowest J values). The CPU requirement of the benchmark-type J > 0 test calculations increases rapidly with the J values, CPU times typically range from one hour to one week (using 32 threads with OpenMP parallelization).

https://doi.org/10.1021/acs.jpca.6c01349
J. Phys. Chem. A 2026, 130, 6312−6326

■ RESULTS AND DISCUSSION

Thermal Reaction Rate Coefficients

The extensive computations of this study have resulted in thermal reaction rate coefficients $k(T)$ for the H_2 + D → HD + H reaction in the temperature range of 75−800 K. All $k(T)$ values shown in Table 2 have been computed with the CCI PES.[117] For half of the reported results, a DBOC-related correction[129] was applied; these $k(T)$ values can be found under the heading 'with barrier correction'. The sets of thermal reaction rate coefficients given in Table 2 are as follows: (a) separate *ortho* and *para* contributions to the thermal reaction rate, $k^{\text{ortho}}(T)$ and $k^{\text{para}}(T)$, respectively; (b) the weighted sum, $k^{\text{full}}(T) = 3\ k^{\text{ortho}}(T) + k^{\text{para}}(T)$, is the reaction rate coefficient that takes into account the contributions from both nuclear spin states (assuming equilibrium between the nuclear spin isomers at all temperatures considered); and (c) the set of extrapolated reaction rate coefficients, $k^{\text{extrapolated}}$. $k^{\text{ortho}}(T)$, $k^{\text{para}}(T)$, and $k^{\text{full}}(T)$ contain only the directly computed $k^J(T)$ contributions up to $J_{\max}$. In clear contrast, $k^{\text{extrapolated}}$ is obtained by including contributions up to $J = 30$, in the sum of eq 6. The $k^J(T)$ values, where $J > J_{\max}$ are obtained by a linear extrapolation (Figure 6, *vide infra*). The linearity relations observed within the computed $k^J(T)$ values, which is utilized during the extrapolation, will be discussed later. Furthermore, Table 2 gives the ratio of $k^{\text{para}}(T)/k^{\text{ortho}}(T)$, which helps illustrate the effect of nuclear spin isomerism on the reaction rate coefficients as a function of temperature. This ratio is different from 1.00 only below 150 K and increases toward lower temperatures. The comparison of the k^{full} and $k^{\text{extrapolated}}$ values in Table 2 serves as a simple convergence test for the choices made for $J_{\max}$ (Table 1). Finally, note that two sets of reaction rate coefficients are tabulated in Table 2 for T = 100 K: one from a direct computation at T = 100 K, and one derived from a computation at T = 200 K, using eq 5 during the evaluation of the flux autocorrelation function, denoted as "100 = 200/2". The agreement of the two values proves the validity of eq 5.

The computed $k(T)$ values obtained with or without the barrier correction[129] are significantly different at the lowest temperatures. A similar result was obtained by Mielke and co-workers,[129] who listed a difference of 34% for their $k(T)$ values calculated at 167 K. At lower temperatures, the correction is even larger; at 75 K, the correction becomes a factor of 2.5. The employed simple barrier correction formula assumes that the reaction rate coefficient is proportional to $e^{-\beta \Delta E_b}$, where ΔE_b is the correction to the barrier height.[129] At the lowest temperatures, this assumption seems to fail, suggesting that more sophisticated schemes should be used to include the DBOC effect. The effect of DBOC on the dynamics of the D + H_2(v = 4, j = 0) reaction was studied in ref 107. This study is not directly relevant to the present paper, nevertheless, it shows that for such light systems, the DBOC correction is not negligible. Other works worth mentioning investigated effects due to the conical intersection between the two lowest electronic states and the geometric phase for the H_2 + H reaction and its isotopic analogues.[158−160]

Figure 2 contains Arrhenius plots of the computed thermal reaction rate coefficients of this study, along with measured[69,71,74,82] and computed[131] values. Clearly, and not surprisingly, the results of this study are in good agreement

Table 2. Thermal Reaction Rate Coefficients $k(T)$, in cm^3 $molecule^{-1}$ s^{-1}, Calculated at Different Temperatures T, with and without a Barrier Correction due to the Diagonal Born−Oppenheimer Correction (DBOC)[129] for the Reaction H_2 + D → HD + H

	Without barrier correction					With barrier correction				
T/K	$k^{\text{ortho}}(T)$	$k^{\text{para}}(T)$	$k^{\text{para}}/k^{\text{ortho}}$	k^{full}	$k^{\text{extrapolated}}$	$k^{\text{ortho}}(T)$	$k^{\text{para}}(T)$	$k^{\text{para}}/k^{\text{ortho}}$	k^{full}	$k^{\text{extrapolated}}$
75	3.4986×10^{-23}	5.3614×10^{-23}	1.53	1.5857×10^{-22}	1.5886×10^{-22}	1.3768×10^{-23}	2.1098×10^{-23}	1.53	6.2400×10^{-23}	6.2515×10^{-23}
100	2.8802×10^{-22}	3.2810×10^{-22}	1.14	1.1922×10^{-21}	1.1984×10^{-21}	1.4310×10^{-22}	1.6301×10^{-22}	1.14	5.9231×10^{-22}	5.9540×10^{-22}
100 = 200/2	2.8924×10^{-22}	3.2995×10^{-22}	1.14	1.1977×10^{-21}	1.1996×10^{-21}	1.4371×10^{-22}	1.6393×10^{-22}	1.14	5.9505×10^{-22}	5.9600×10^{-22}
150	1.7061×10^{-20}	1.7104×10^{-20}	1.00	6.8288×10^{-20}	6.9362×10^{-20}	1.0703×10^{-20}	1.0730×10^{-20}	1.00	4.2837×10^{-20}	4.3511×10^{-20}
200	6.4825×10^{-19}	6.4836×10^{-19}	1.00	2.5931×10^{-18}	2.6292×10^{-18}	4.5693×10^{-19}	4.5701×10^{-19}	1.00	1.8278×10^{-18}	1.8533×10^{-18}
300	9.2821×10^{-17}	9.2833×10^{-17}	1.00	3.7130×10^{-16}	3.7326×10^{-16}	7.3517×10^{-17}	7.3527×10^{-17}	1.00	2.9408×10^{-16}	2.9563×10^{-16}
400	1.6119×10^{-15}	1.6123×10^{-15}	1.00	6.4480×10^{-15}	6.4482×10^{-15}	1.3533×10^{-15}	1.3536×10^{-15}	1.00	5.4135×10^{-15}	5.4136×10^{-15}
800	1.7385×10^{-13}	1.7387×10^{-13}	1.00	6.9541×10^{-13}	6.9846×10^{-13}	1.5929×10^{-13}	1.5931×10^{-13}	1.00	6.3719×10^{-13}	6.3999×10^{-13}

https://doi.org/10.1021/acs.jpca.6c01349
J. Phys. Chem. A 2026, 130, 6312−6326

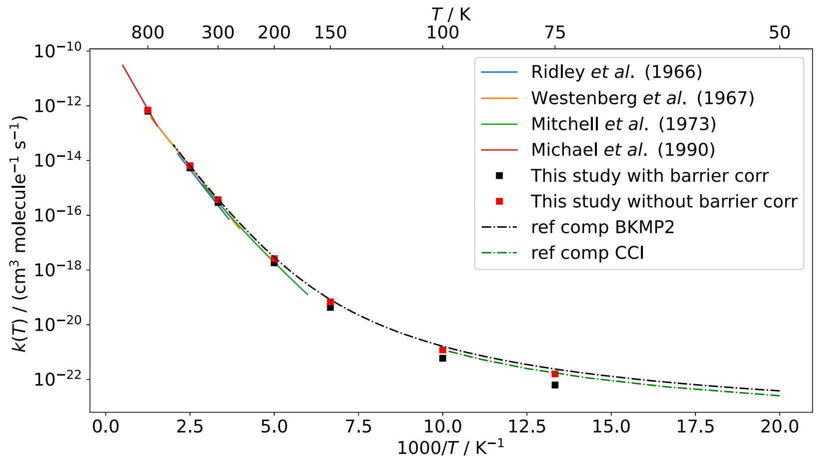

Figure 2. Arrhenius plot of the computed thermal reaction rate coefficients with and without the barrier correction, along with measured[69,71,74,82] values (solid lines), and literature data[131] computed on the BKMP2 and CCI PESs (dash-dotted lines). The measured data are plotted as the Arrhenius fits of ref 129.

Table 3. First Eight Thermal Flux (J = 0) Eigenvalues, Given in Atomic Units (a.u.), at Three Different Temperatures[a]

Index	Symm.	150 K	300 K	800 K
1,2	even	$\pm1.4943 \times 10^{-19}$	$\pm2.4363 \times 10^{-13}$	$\pm9.8967 \times 10^{-8}$
3,4	odd	$\pm1.3296 \times 10^{-19}$	$\pm2.4296 \times 10^{-13}$	$\pm9.8967 \times 10^{-8}$
5,6	odd	$\pm7.4917 \times 10^{-21}$	$\pm8.6659 \times 10^{-15}$	$\pm9.5108 \times 10^{-9}$
7,8	even	$\pm8.7008 \times 10^{-21}$	$\pm8.6796 \times 10^{-15}$	$\pm9.5114 \times 10^{-9}$

[a]The column Symm. specifies the symmetry of thermal flux eigenstates under the permutation of the two hydrogen atoms.

with the experimental values from all four sources and with earlier theoretical results. For a reaction studied from very low (near 0 K) to very high temperatures, the Arrhenius plot, that is $\ln k(T)$ vs. $1/T$, is expected to show the following shape: straight at high temperatures (no observable effect from tunneling), flat at very low temperatures (when the reaction proceeds strictly due to tunneling, the rate is independent of the temperature for exothermic reactions), and curved in between. Some of this expected behavior can be observed in Figure 2, even in the slopes of the experimental measurements conducted at different temperature ranges. It is also clear that the tunneling regime is not approached closely at 75 K, the lowest temperature point of this study. As estimated in ref 93, for the H_2 + D → HD + H reaction, the flat regime should be visible below about 10 K.

While the computed $k(T)$ values are of primary interest for reaction kinetics, it is equally important, from methodological and computational points of view, to discuss some of the intermediate computational results leading to the thermal reaction rate coefficients. These important aspects of the present study are elaborated in the next subsections.

Thermal Flux Eigensystem

Due to the fact that the thermal flux operator is purely imaginary and Hermitian, $\hat{F}(\beta)^* = -\hat{F}(\beta)$, its eigenvalues come in ± pairs, and the corresponding eigenvectors are complex conjugates of one another. The first few highest (in absolute value) thermal flux eigenvalues of the H_2 + D → HD + H reaction with the J = 0 constraint are given in Table 3 at a few selected temperatures. The most notable qualitative feature of the data is that, at higher temperatures, quasidegenerate pairs of the ± pairs start to appear, yielding eigenvalue quadruplets with close-lying absolute values. This can be explained by the fact that at higher temperatures the two reaction channels become virtually independent. The quasidegeneracy is lost at lower temperatures.

The squared absolute value of the thermal flux J = 0 eigenvectors at T = 300 K is plotted in Figure 3. The two colors in these plots represent the symmetry of the eigenvectors under the permutation of the two indistinguishable hydrogen atoms. The first and seventh eigenvectors, Figure 3a and d, respectively, are symmetric; thus, these are associated with *para* states. The third and fifth eigenvectors, Figure 3b and c, respectively, are antisymmetric; thus, these two are *ortho* states. At higher temperatures, the *ortho* and *para* reaction rate coefficients are virtually equal due to quasidegeneracies in the spectrum of the thermal flux. At lower temperatures, the *ortho* and *para* reaction rate coefficients differ and the quasidegeneracy is lost. It is important to note, however, that the quasidegeneracy of the thermal flux eigenvalues alone is not a quantitative measure of the $k^{\text{para}}/k^{\text{ortho}}$ ratio. For example, while the quasidegeneracy is already lifted at T = 150 K (see Table 3), the $k^{\text{para}}/k^{\text{ortho}}$ ratio is still 1.00. On the other hand, at T = 75 the ratio is 1.53, although the rate coefficients were computed using the T = 150 K thermal flux eigenpairs and eq 5.

Further insight into the eigenstates can be gained from Figure 4, which shows the first thermal flux eigenstate at two different temperatures, T = 100 K and T = 800 K. Clearly, the picture is rather different at the two temperatures. As expected, thermal flux eigenstates are more localized in the vicinity of the transition state at T = 800 K, whereas at T = 100 K, they are located farther away from the transition state, in the reactant and product valleys. Note that the transition state is located at r = 1.7572 a_0, R = 2.6358 a_0, and θ = 0 and 180° for the two reaction channels. Since the barrier between the two channels is high at the transition state, at high temperatures the thermal flux eigenstates can be divided into

https://doi.org/10.1021/acs.jpca.6c01349
J. Phys. Chem. A 2026, 130, 6312−6326

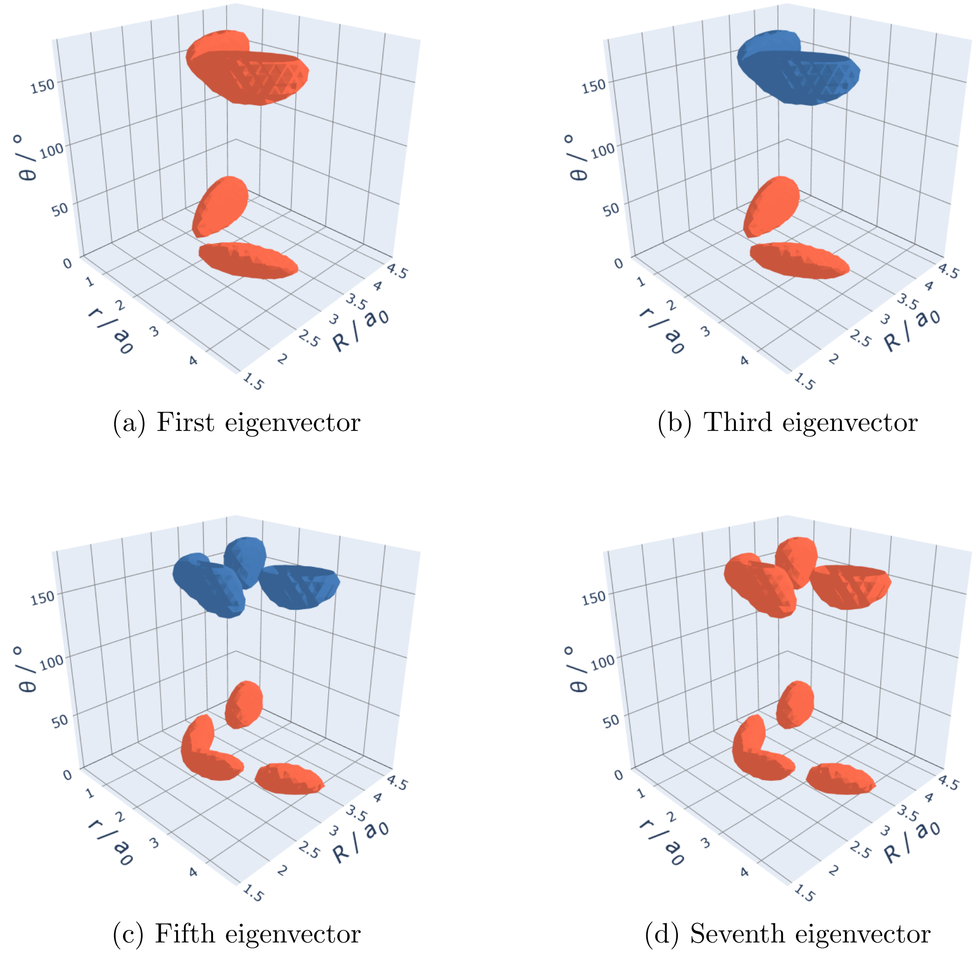

Figure 3. Isosurface plot of the squared absolute value of the first (panel (a)), third (panel (b)), fifth (panel (c)), and seventh (panel (d)) thermal flux eigenvectors for the $J = 0$ $H_2 + D \rightarrow HD + H$ reaction, at $T = 300$ K. Only one of the eigenvectors is plotted for each complex conjugate eigenvector pair. The coloring represents the symmetry of the eigenvectors under the exchange of the two hydrogen atoms. The first and seventh eigenvectors are symmetric, while the third and fifth eigenvectors are antisymmetric under the $\theta \rightarrow \pi - \theta$ transformation, that is, the permutation of the two hydrogen atoms.

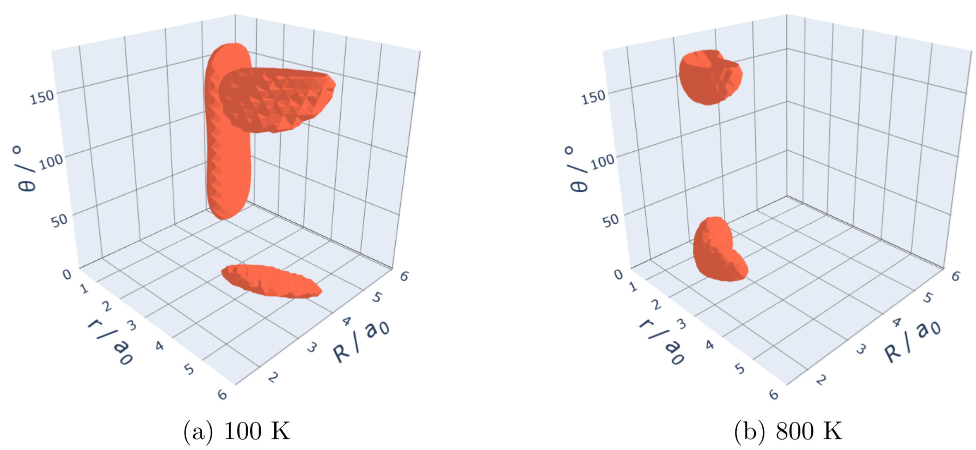

Figure 4. Isosurface plot of the squared absolute value of the first eigenstate (symmetric under the exchange of the two hydrogen atoms, *para*) of the thermal flux at two different temperatures (panel (a): $T = 100$ K, panel (b): $T = 800$ K).

two noninteracting parts, each for the two reaction channels, causing the quasidegeneracy in the thermal flux eigenvalues (see Table 3). However, at distances far from the transition state in the reactant channel, the barrier between the two channels decreases. Therefore, as the thermal flux eigenstates leave the transition state region as the temperature decreases, they reach regions where the barrier is no longer high enough to prevent the interaction between the two channels; thus, the degeneracy is lifted in the eigenvalues and the *ortho* and *para* reaction rate coefficients eventually start to differ.

https://doi.org/10.1021/acs.jpca.6c01349
J. Phys. Chem. A 2026, 130, 6312−6326

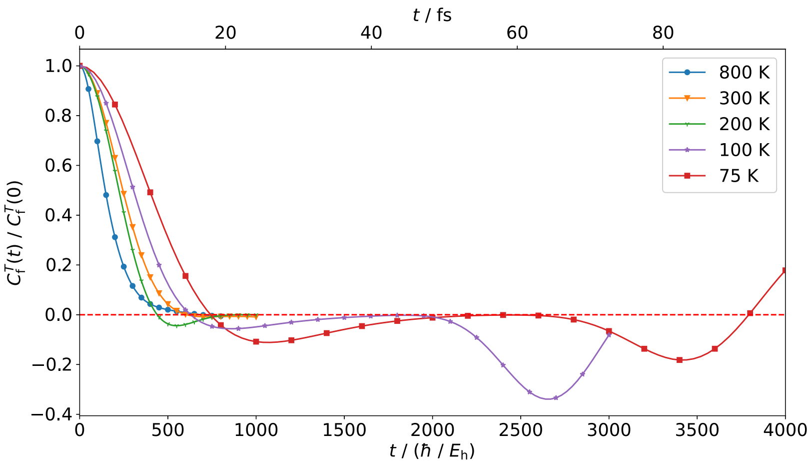

Figure 5. Flux autocorrelation function summed for all relevant J and nuclear spin states, normalized by its value at $t = 0$, and plotted for a few selected temperatures as a function of time. All flux autocorrelation functions converge to zero; thus, an appropriate integration upper bound can be chosen. The diverging tails, see, e.g., $t > 2000\ \hbar/E_h$ for $T = 100$ K, are caused by unphysical reflection from the end of the DVR grid.

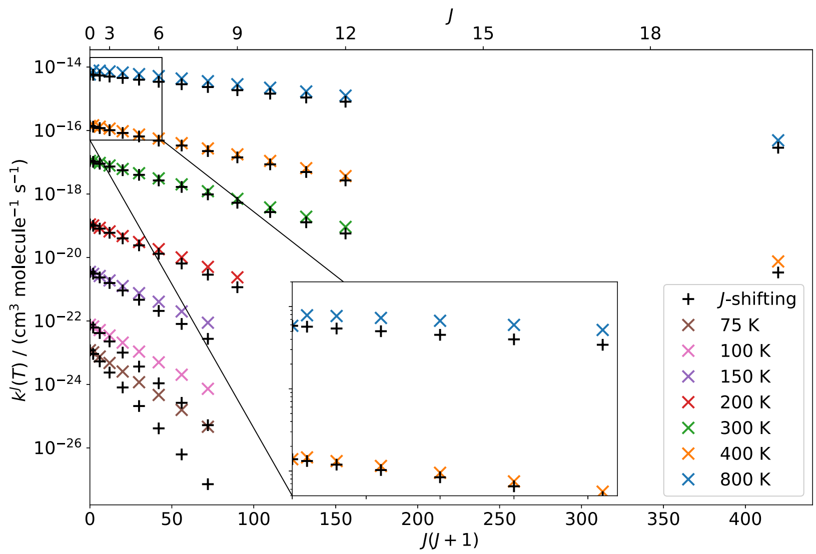

Figure 6. Semilog plot of the $k^J(T)$ contributions to the full $k(T)$ value as a function of $J(J + 1)$ at temperatures between 75 and 800 K. Thermal rate coefficients obtained by the J-shifting approximation are also shown. The deviations observed at low temperatures are caused by the change of the effective rotational constant, while at high temperatures they can be attributed to non-negligible $K \neq 0$ contributions for low J values (see the inset).

Flux Autocorrelation Functions

Figure 5 shows the flux autocorrelation function $C_f^T(t)$ at a few selected temperatures. The functions are normalized by their value at $t = 0$; otherwise, they would differ by several orders of magnitude. All functions converge to zero eventually; however, the autocorrelation functions at lower temperatures converge at a slower rate, as expected. At certain temperatures, diverging tails can be observed. These unphysical parts of the flux autocorrelation function are caused by the reflection of the thermal flux eigenstates from the end of the grid during the real time evolution. A complex absorbing potential (CAP) could avoid such reflections; however, in the current study, we avoided the use of a CAP since all the flux autocorrelation functions converged to zero before the reflections emerged.

Rotational Effects

The different computed $k^J(T)$ contributions are plotted in Figure 6 as a function of $J(J + 1)$ at all the temperatures chosen for the $k(T)$ computations. The rotational contributions computed using the J-shifting approximation are also shown. Within the J-shifting approximation, $k^J(T)$ can be obtained as

$$k^J(T) = k^{J=0}(T)e^{-\beta E_J^{\ddagger}} \tag{15}$$

where $E_J^{\ddagger}$ is the rigid-rotor rotational energy of the reactive system at the transition-state geometry. Since, in the case of the H_2 + D → HD + H reaction, the transition-state structure is linear, the energy level formula $E_J^{\ddagger} = B^{\ddagger}J(J + 1)$ applies with $B^{\ddagger}$ = 7.04 cm^{-1}. Therefore, the log $k^J(T) - J(J + 1)$ plot is linear within the J-shifting approximation (see Figure 6). Remarkably, exactly computed $k^J(T)$ values show a similar behavior, deviating from linearity only at high temperatures for low J values (see the inset in Figure 6), due to non-negligible $K \neq 0$ contributions. As is clear from Figure 6, the slopes of exact $k^J(T)$ values and the J-shifting ones are virtually equal at high temperatures, while they deviate at low temperatures. The exact values of the slopes are tabulated in

https://doi.org/10.1021/acs.jpca.6c01349
J. Phys. Chem. A 2026, 130, 6312−6326

Table 4. Effective rotational constants B^{eff} can be computed from the slope of the exact $k^J(T)$ values for each temperature, these rotational constants can also be found in Table 4. At higher temperatures, B^{eff} is in good agreement with $B^{\ddagger}$. As the temperature is reduced, B^{eff} decreases appreciably and as a consequence, the deviation between B^{eff} and $B^{\ddagger}$ increases. These findings suggest that the effective linear transition-state structure consistent with B^{eff} is temperature dependent. Moreover, a decrease in B^{eff} implies that the bonds of the effective transition-state structure are elongated at lower temperatures. We believe that this observation is in line with the fact that thermal flux eigenstates leave the transition state region as the temperature is reduced (see Figure 4).

■ CONCLUSIONS

Ever since the ground-breaking, classic studies of Eyring, Evans, and Polanyi,[5−7] the various statistical, classical, semiclassical, and quantum approaches developed have helped explain several characteristic observations in chemical kinetics, among them (a) general trends in the preexponential factors of the Arrhenius equation, (b) kinetic isotope effects of bimolecular reactions, (c) the temperature dependence of thermal reaction rate coefficients, (d) the role of quantum effects (zero-point vibrations, tunneling, identical particle symmetry, resonances, interference, the still somewhat exotic Aharonov−Bohm effect[161]), and (e) deviations of certain reactions even from the generalized Arrhenius form of the rate equation. One of the principal aims of the present study was to provide an improved implementation of a direct quantum mechanical algorithm based on flux autocorrelation, applicable for the efficient computation of thermal reaction rate coefficients. The methodology was tested on the prototypical H_2 + D → HD + H reaction over the wide temperature range of 75−800 K.

There are several characteristics of the improved methodology worth emphasizing. First, it is the strong belief of the authors that the combination of the fully numerical formulation of the rovibrational Hamiltonian allowed within the GENIUSH approach with the "direct" method, originally developed by Yamamoto, Miller, and Manthe, provides a unique opportunity to develop a black-box-type approach for the computation of thermal reaction rate coefficients. GENIUSH can construct the exact and general rovibrational Hamiltonian for arbitrary molecules, internal coordinates, and body-fixed frame embeddings with little effort on the user's side; most importantly, no analytical form of the kinetic energy operator is needed. Thus, the GENIUSH approach is useful not only for obtaining time-independent rovibrational energy levels and eigenstates,[137] but also for describing the rate of chemical reactions. It should also be mentioned that GENIUSH has already been used for a time-dependent quantum dynamics study.[162] Second, the flexibility of choosing any internal coordinates and embeddings in GENIUSH facilitates symmetry considerations for equivalent nuclei, which can reduce the computational cost and help enforce the Pauli exclusion principle. Third, reduced-dimensional models are easy to implement in GENIUSH, which can find application for the quantum mechanical description of larger systems, especially if there are internal degrees of freedom that are less relevant for the chemical reaction under investigation.

Table 4. Slopes of the Curves in Figure 6 Obtained by Fitting a Line to the Last Two Data Points as well as Computed Using the *J*-Shifting Approximation, and Effective Rotational Constants Derived from the Fitted Slopes

T/K	B^{eff}/cm^{-1}	fitted	*J*-shifting
75	3.98	−0.07632	−0.13499
100	4.43	−0.06380	−0.10124
150	5.31	−0.05097	−0.06749
200	5.87	−0.04226	−0.05062
300	6.43	−0.03082	−0.03375
400	6.52	−0.02346	−0.02531
800	6.83	−0.01229	−0.01266

In the current work, GENIUSH has been applied to the H_2 + D → HD + H reaction, performing numerically exact full-dimensional computations that include rotational and nuclear spin degrees of freedom as well. Due to numerical issues experienced with the Podolsky form of the general rovibrational kinetic energy operator used extensively in earlier work, we had to devise a new form of the kinetic energy (termed the partially rearranged form) to obtain correct reaction rate coefficients. The H_2 + D → HD + H reaction, studied both experimentally and theoretically in great detail, provided an outstanding testing ground for our algorithm. Excellent agreement with earlier experimental and computational results has been achieved by the current work in a broad temperature range for the H_2 + D → HD + H reaction. In addition, we have also presented interesting results related to rotational effects and nuclear spin (such as the temperature dependence of the ratio k^{para}/k^{ortho}).

We envision that the algorithm and the code developed and described in this paper will allow for the computation of thermal reaction rate coefficients for significantly larger systems than the triatomic test system examined here. One possible direction is the investigation of chemical reactions that cannot accurately be described by the most commonly used classical and semiclassical methods due to the importance of quantum effects. Such effects are particularly relevant in reactions involving light atoms and occurring at low temperatures—conditions commonly encountered in astrochemical environments.

■ APPENDIX PARTIALLY REARRANGED FORM OF THE EXACT KINETIC ENERGY OPERATOR

In most computations of rovibrational energy levels and eigenstates utilizing the GENIUSH code,[42,43] the Podolsky form[39] of the exact kinetic energy operator has been used. The most time-consuming part of a rovibrational computation is the determination of the required energy levels and eigenstates of the rovibrational Hamiltonian matrix **H**, which is carried out by the iterative Lanczos algorithm[145] in GENIUSH.

To this end, the matrix representation of the Hamiltonian is set up in a multidimensional direct-product DVR basis, and matrix-vector products **Hv** are evaluated by an efficient algorithm that exploits the sparsity of **H**. **H** is constructed by inserting resolutions of identity between the different operators in the Podolsky form of the kinetic energy (see eq 10). This procedure provides numerically exact bound rovibrational energy levels and wave functions. Unfortunately, serious numerical issues arise if the Podolsky form is applied

https://doi.org/10.1021/acs.jpca.6c01349
J. Phys. Chem. A 2026, 130, 6312−6326

to compute bimolecular reaction rate coefficients using the resolution-of-identity approach.

For the sake of simplicity, let us assume that the quantities $\tilde{g}$ and G_{kl} do not depend on the internal coordinates, and a single vibrational degree of freedom is considered. In this case, the vibrational kinetic energy is equal to

$$\hat{T}^{\mathrm{vib}} = -\frac{\hbar^2}{2}\frac{\mathrm{d}}{\mathrm{d}q}G\frac{\mathrm{d}}{\mathrm{d}q} \tag{16}$$

where G is a constant and q is the vibrational coordinate. Using the resolution-of-identity approach, we get

$$\mathbf{T}^{\mathrm{vib,res}} = -\frac{\hbar^2}{2}G\mathbf{D}^{(1)}\mathbf{D}^{(1)} \tag{17}$$

where $\mathbf{D}^{(1)}$ is the matrix representation of the first derivative operator. Without inserting a resolution of identity between the two derivative operators, one would get

$$\mathbf{T}^{\mathrm{vib}} = -\frac{\hbar^2}{2}G\mathbf{D}^{(2)} \tag{18}$$

where $\mathbf{D}^{(2)}$ denotes the second derivative matrix. The two approaches yield nearly identical results if $\mathbf{D}^{(2)}$ is well approximated by $\mathbf{D}^{(1)}\mathbf{D}^{(1)}$.

The difference between $\mathbf{D}^{(1)}\mathbf{D}^{(1)}$ and $\mathbf{D}^{(2)}$ is shown in Figure 7 for a basis of 40 sine-DVR functions. The difference matrix has large elements (in absolute value) at its top left and bottom right corners, corresponding to DVR points at the two edges of the grid. Thus, the approximation $\mathbf{D}^{(2)} \approx \mathbf{D}^{(1)}\mathbf{D}^{(1)}$ is inaccurate at the edges of the grid and accurate in the middle region. If more DVR grid points are used, the central matrix elements of $\left|\mathbf{D}^{(1)}\mathbf{D}^{(1)} - \mathbf{D}^{(2)}\right|$ become smaller, eventually approaching zero, while the matrix elements at the edges never vanish, regardless of the grid size. Such errors are irrelevant if bound states with zero amplitude at the edges of the grid are considered. However, if $\hat{F}(\beta)$ is to be diagonalized for a bimolecular reaction, the edges of the grid are highly relevant. Thus, the insertion of a resolution of identity between the derivative operators causes severe numerical errors.

To obtain correct thermal reaction rate coefficients, it is necessary to rearrange the rovibrational kinetic energy operator. In the partially rearranged form of eq 11, diagonal ($k = l$) terms in the vibrational kinetic energy operator, where a resolution of identity would normally be inserted between the two first-derivative operators $\partial/\partial q_k$, are rearranged so that, in the final form, a second-derivative operator appears instead of two first-derivative operators. A somewhat similar rearrangement was performed in ref 46; however, it was applied to an already rearranged form of the rovibrational kinetic energy operator and not to the Podolsky form.

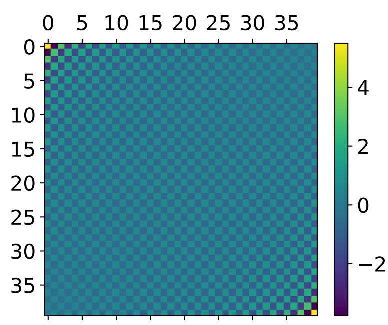

Figure 7. Graphical representation of the elements of the $\mathbf{D}^{(1)}\mathbf{D}^{(1)} - \mathbf{D}^{(2)}$ matrix (see eqs 17 and 18), based on 40 sine-DVR points. The differences become large (in absolute value) at the top left and bottom right corners of the difference matrix. Consequently, the resolution-of-identity approximation causes the largest errors at the boundaries of the grid.

The partially rearranged form of $\hat{T}^{\mathrm{vib}}$ is Hermitian. However, depending on the numerical approach, the matrix representation of $\hat{T}^{\mathrm{vib}}$ is not necessarily Hermitian. In GENIUSH, resolutions of identity are inserted into eq 11 between $\partial(G_{kk}\tilde{g}^{1/2})/\partial q_k$ and $\partial/\partial q_k$, and between $G_{kk}\tilde{g}^{1/2}$ and $\partial^2/\partial q_k^2$. Let us define $\mathbf{A}_{kk}$ and $\mathbf{A}'_{kk}$ as the matrix representations of $G_{kk}\tilde{g}^{1/2}$ and $\partial(G_{kk}\tilde{g}^{1/2})/\partial q_k$ in DVR, respectively, and denote derivative matrices of the kth vibrational degree of freedom by $\mathbf{D}_k^{(1)}$ and $\mathbf{D}_k^{(2)}$. Using this notation, we get

$$\begin{aligned}(\mathbf{A}'_{kk}\mathbf{D}_k^{(1)} + \mathbf{A}_{kk}\mathbf{D}_k^{(2)})^{\dagger} &= (\mathbf{D}_k^{(1)})^{\mathrm{T}}(\mathbf{A}'_{kk})^{\mathrm{T}} + (\mathbf{D}_k^{(2)})^{\mathrm{T}}\mathbf{A}_{kk}^{\mathrm{T}} \\ &= (\mathbf{D}_k^{(1)})^{\mathrm{T}}\mathbf{A}'_{kk} + (\mathbf{D}_k^{(2)})^{\mathrm{T}}\mathbf{A}_{kk} \\ &\neq \mathbf{A}'_{kk}\mathbf{D}_k^{(1)} + \mathbf{A}_{kk}\mathbf{D}_k^{(2)}\end{aligned} \tag{19}$$

where the adjoint was replaced by the transpose since all matrices are real-valued, and $\mathbf{A}_{kk}$ and $\mathbf{A}'_{kk}$ are diagonal in a DVR basis, thus symmetric. $\mathbf{D}_k^{(1)}$ and $\mathbf{D}_k^{(2)}$ are usually antisymmetric and symmetric, respectively, for most DVR basis types; however, in general, this is not true. The matrix representation of the kinetic energy operator should be Hermitian; thus, eq 19 must be symmetrized as follows:

$$(\mathbf{A}'_{kk}\mathbf{D}_k^{(1)} + \mathbf{A}_{kk}\mathbf{D}_k^{(2)} + (\mathbf{D}_k^{(1)})^{\mathrm{T}}\mathbf{A}'_{kk} + (\mathbf{D}_k^{(2)})^{\mathrm{T}}\mathbf{A}_{kk})/2 \tag{20}$$

Note that such symmetrization is not needed in the off-diagonal terms ($k \neq l$) of $\hat{T}^{\mathrm{vib}}$, since the two first derivative operators $\partial/\partial q_k$ and $\partial/\partial q_l$ act on different degrees of freedom. In this case, the resolution of identity can be safely inserted between $\partial/\partial q_k$ and $\partial/\partial q_l$. The cost of matrix-vector multiplication is increased because of the symmetrization. However, since it is only needed in the diagonal ($k = l$) terms of $\hat{T}^{\mathrm{vib}}$, and the time complexity of the matrix-vector multiplication algorithm remains unchanged, the cost increment caused by the symmetrization is manageable. Thus, the final symmetrized matrix representation of the partially rearranged operator $\hat{T}^{\mathrm{vib}}$ reads as

$$\begin{aligned}\mathbf{T}^{\mathrm{vib}} = {} & \frac{\hbar^2}{2}\sum_{k\neq l}^{D}\tilde{\mathbf{g}}^{-1/4}(\mathbf{D}_k^{(1)})^{\mathrm{T}}\mathbf{A}_{kl}\mathbf{D}_l^{(1)}\tilde{\mathbf{g}}^{-1/4} \\ & - \frac{\hbar^2}{4}\sum_{k=1}^{D}\tilde{\mathbf{g}}^{-1/4}(\mathbf{A}'_{kk}\mathbf{D}_k^{(1)} + \mathbf{A}_{kk}\mathbf{D}_k^{(2)} + (\mathbf{D}_k^{(1)})^{\mathrm{T}}\mathbf{A}'_{kk} \\ & + (\mathbf{D}_k^{(2)})^{\mathrm{T}}\mathbf{A}_{kk})\tilde{\mathbf{g}}^{-1/4}\end{aligned} \tag{21}$$

which is now implemented in GENIUSH.

■ AUTHOR INFORMATION

Corresponding Author

Csaba Fábri − *Department of Theoretical Physics, University of Debrecen, H-4002 Debrecen, Hungary;* orcid.org/

https://doi.org/10.1021/acs.jpca.6c01349
J. Phys. Chem. A 2026, 130, 6312−6326

0000-0001-9746-1548; Email: fabri.csaba@science.unideb.hu

Authors

Gábor A. Ecseri − *Institute of Chemistry, ELTE Eötvös Loránd University, H-1117 Budapest, Hungary; ELTE Hevesy György PhD School of Chemistry, H-1117 Budapest, Hungary*

Attila G. Császár − *Institute of Chemistry, ELTE Eötvös Loránd University, H-1117 Budapest, Hungary*

Complete contact information is available at: https://pubs.acs.org/10.1021/acs.jpca.6c01349

Notes

The authors declare no competing financial interest.

■ ACKNOWLEDGMENTS

This paper is dedicated to the late Professor John F. Stanton, a friend and colleague with whom the second author (A.G.C.) has enjoyed numerous stimulating discussions about theoretical and computational chemistry, resulting in several joint publications. The project described received funding from the National Research, Development, and Innovation Office of Hungary (NKFIH, grants no. 152791 and K146096). This paper was supported by the János Bolyai Research Scholarship of the Hungarian Academy of Sciences.

■ REFERENCES

(1) Eckart, C. The penetration of a potential barrier by electrons. *Phys. Rev.* **1930**, *35*, 1303−1309.
(2) Marcus, R. A. Unimolecular dissociations and free radical recombination reactions. *J. Chem. Phys.* **1952**, *20*, 359−364.
(3) Miller, W. H. Quantum mechanical transition state theory and a new semiclassical model for reaction rate constants. *J. Chem. Phys.* **1974**, *61*, 1823−1834.
(4) Miller, W. H. Semiclassical limit of quantum mechanical transition state theory for nonseparable systems. *J. Chem. Phys.* **1975**, *62*, 1899−1906.
(5) Eyring, H.; Polanyi, M. Über einfache Gasreaktionen. *Z. Phys. Chem. B* **1931**, *12*, 279−311.
(6) Eyring, H. The activated complex in chemical reactions. *J. Chem. Phys.* **1935**, *3*, 107−115.
(7) Evans, M. G.; Polanyi, M. Some applications of the transition state method to the calculation of reaction velocities, especially in solution. *Trans. Faraday Soc.* **1935**, *31*, 875−894.
(8) Wigner, E. The transition state method. *Trans. Faraday Soc.* **1938**, *34*, 29.
(9) Eliason, M. A.; Hirschfelder, J. O. General collision theory treatment for the rate of bimolecular, gas phase reactions. *J. Chem. Phys.* **1959**, *30*, 1426−1436.
(10) Truhlar, D. G.; Hase, W. L.; Hynes, J. T. Current status of transition-state theory. *J. Phys. Chem. A* **1983**, *87*, 2664−2682.
(11) Truhlar, D. G.; Garrett, B. C. Variational transition state theory. *Annu. Rev. Phys. Chem.* **1984**, *35*, 159−189.
(12) Truhlar, D. G.; Garrett, B. C.; Klippenstein, S. Current status of transition-state theory. *J. Phys. Chem. A* **1996**, *100*, 12771−12800.
(13) Laidler, K. J.; King, M. C. Development of transition-state theory. *J. Phys. Chem. A* **1983**, *87*, 2657−2664.
(14) Child, M. S. *Molecular Collision Theory*; Dover: Mineola, NY, 1996.
(15) McQuarrie, D. A.; Simon, J. D. *Physical Chemistry: A Molecular Approach*; University Science Books, 1997.
(16) Schatz, G. C.; Ratner, M. A. *Quantum Mechanics in Chemistry*; Dover, New York, 2002.
(17) Chapman, S.; Cowling, T. G. *The Mathematical Theory of Non-Uniform Gases*, 3rd ed.; Cambridge University Press: Cambridge, 1970.
(18) Welsch, R.; Manthe, U. Thermal flux based analysis of state-to-state reaction probabilities. *Mol. Phys.* **2012**, *110*, 703−715.
(19) Yamamoto, T. Quantum statistical mechanical theory of the rate of exchange chemical reactions in the gas phase. *J. Chem. Phys.* **1960**, *33*, 281−289.
(20) Miller, W. H.; Schwartz, S. D.; Tromp, J. W. Quantum mechanical rate constants for bimolecular reactions. *J. Chem. Phys.* **1983**, *79*, 4889−4898.
(21) Miller, W. H. Semiclassical methods in chemical physics. *Science* **1986**, *233*, 171−177.
(22) Seideman, T.; Miller, W. H. Transition state theory, Siegert eigenstates, and quantum mechanical reaction rates. *J. Chem. Phys.* **1991**, *95*, 1768−1780.
(23) Miller, W. H. Beyond transition-state theory: A rigorous quantum theory of chemical reaction rates. *Acc. Chem. Res.* **1993**, *26*, 174−181.
(24) Wang, H.; Thompson, W. H.; Miller, W. H. "Direct" calculation of thermal rate constants for the F + H_2 → HF + F reaction. *J. Phys. Chem. A* **1998**, *102*, 9372−9379.
(25) Manthe, U. A new time-dependent approach to the direct calculation of reaction rates. *J. Chem. Phys.* **1995**, *102*, 9205−9213.
(26) Manthe, U.; Matzkies, F. Quantum calculations of thermal rate constants and reaction probabilities: H_2 + CN → H + HCN. *Chem. Phys. Lett.* **1998**, *282*, 442−449.
(27) Matzkies, F.; Manthe, U. Accurate quantum calculations of thermal rate constants employing MCTDH: H_2 + OH → H + H_2O and D_2 + OH → D + DOH. *J. Chem. Phys.* **1998**, *108*, 4828−4836.
(28) Matzkies, F.; Manthe, U. Combined iterative diagonalization and statistical sampling in accurate reaction rate calculations: Rotational effects in O + HCl → OH + Cl. *J. Chem. Phys.* **2000**, *112*, 130−136.
(29) Huarte-Larrañaga, F.; Manthe, U. Thermal rate Constants for polyatomic reactions: First principles quantum Theory. *Z. Phys. Chem.* **2007**, *221*, 171−213.
(30) Manthe, U. Accurate calculations of reaction rates: predictive theory based on a rigorous quantum transition state concept. *Mol. Phys.* **2011**, *109*, 1415−1426.
(31) Welsch, R.; Huarte-Larrañaga, F.; Manthe, U. State-to-state reaction probabilities within the quantum transition state framework. *J. Chem. Phys.* **2012**, *136*, 064117.
(32) Zhang, D. H.; Light, J. C. Cumulative reaction probability via transition state wave packets. *J. Chem. Phys.* **1996**, *104*, 6184−6191.
(33) Miller, S. M.; Carrington, T. Calculation of reaction probabilities using wavepackets. *Chem. Phys. Lett.* **1997**, *267*, 417−421.
(34) Runge, K.; Cory, M. G.; Bartlett, R. J. The calculation of thermal rate constants for gas phase reactions: A semiclassical flux−flux autocorrelation function (SCFFAF) approach. *J. Chem. Phys.* **2001**, *114*, 5141−5148.
(35) Medvedev, D. M.; Gray, S. K. A new expression for the direct quantum mechanical evaluation of the thermal rate constant. *J. Chem. Phys.* **2004**, *120*, 9060−9070.
(36) Ke, Y.; Kaspar, C.; Erpenbeck, A.; Peskin, U.; Thoss, M. Nonequilibrium reaction rate theory: Formulation and implementation within the hierarchical equations of motion approach. *J. Chem. Phys.* **2022**, *157*, 034103.
(37) Dupuy, L.; Lauvergnat, D.; Scribano, Y. Smolyak representations with absorbing boundary conditions for reaction path Hamiltonian model of reactive scattering. *Chem. Phys. Lett.* **2022**, *787*, 139241.
(38) Miller, W. H. "Direct" and "correct" calculation of canonical and microcanonical rate constants for chemical reactions. *J. Phys. Chem. A* **1998**, *102*, 793−806.
(39) Podolsky, B. Quantum-mechanically correct form of Hamiltonian function for conservative systems. *Phys. Rev.* **1928**, *32*, 812−816.

(40) Louck, J. D.; Galbraith, H. W. Eckart vectors, Eckart frames, and polyatomic molecules. *Rev. Mod. Phys.* **1976**, *48*, 69−106.
(41) Mátyus, E.; Czakó, G.; Sutcliffe, B. T.; Császár, A. G. Vibrational energy levels with arbitrary potentials using the Eckart−Watson Hamiltonians and the discrete variable representation. *J. Chem. Phys.* **2007**, *127*, 084102.
(42) Mátyus, E.; Czakó, G.; Császár, A. G. Toward black-box-type full- and reduced-dimensional variational (ro)vibrational computations. *J. Chem. Phys.* **2009**, *130*, 134112.
(43) Fábri, C.; Mátyus, E.; Császár, A. G. Rotating full- and reduced-dimensional quantum chemical models of molecules. *J. Chem. Phys.* **2011**, *134*, 074105.
(44) Pesonen, J. Eckart frame vibration-rotation Hamiltonians: Contravariant metric tensor. *J. Chem. Phys.* **2014**, *140*, 074101.
(45) Szalay, V. Understanding nuclear motions in molecules: derivation of Eckart frame ro-vibrational Hamiltonian operators *via* a gateway Hamiltonian operator. *J. Chem. Phys.* **2015**, *142*, 174107.
(46) Avila, G.; Mátyus, E. Full-dimensional (12D) variational vibrational states of $CH_4{\cdot}F^-$: Interplay of anharmonicity and tunneling. *J. Chem. Phys.* **2019**, *151*, 154301.
(47) Park, T. J.; Light, J. C. Quantum calculation of thermal rate constants for the H + D_2 reaction. *J. Chem. Phys.* **1992**, *96*, 8853−8862.
(48) Bowman, J. M. Reduced dimensionality theory of quantum reactive scattering. *J. Phys. Chem. A* **1991**, *95*, 4960−4968.
(49) Bowman, J. Overview of reduced dimensionality quantum approaches to reactive scattering. *Theor. Chem. Acc.* **2002**, *108*, 125−133.
(50) Qi, J.; Bowman, J. M. A test of *J*-shifting for H + CO recombination. *Chem. Phys. Lett.* **1997**, *276*, 371−374.
(51) Xie, T.; Bowman, J. M.; Peterson, K. A.; Ramachandran, B. Quantum calculations of the rate constant for the $O(^3P)$+HCl reaction on new *ab initio* $^3A''$ and $^3A'$ surfaces. *J. Chem. Phys.* **2003**, *119*, 9601−9608.
(52) Pack, R. T. Space-fixed vs body-fixed axes in atom-diatomic molecule scattering. Sudden approximations. *J. Chem. Phys.* **1974**, *60*, 633−639.
(53) McGuire, P.; Kouri, D. J. Quantum mechanical close coupling approach to molecular collisions. j_z conserving coupled states approximation. *J. Chem. Phys.* **1974**, *60*, 2488−2499.
(54) Petty, C.; Poirier, B. Comparison of *J*-shifting models for rovibrational spectra as applied to the HO_2 molecule. *Chem. Phys. Lett.* **2014**, *605-606*, 16−21.
(55) Sarka, J.; Poirier, B.; Szalay, V.; Császár, A. G. On neglecting Coriolis and related couplings in first-principles rovibrational spectroscopy: considerations of symmetry, accuracy, and simplicity. *Sci. Rep.* **2020**, *10*, 4872.
(56) Truhlar, D. G.; Wyatt, R. E. History of H_3 kinetics. *Annu. Rev. Phys. Chem.* **1976**, *27*, 1−43.
(57) Truhlar, D. G.; Wyatt, R. E. H + H_2: Potential-energy surfaces and elastic and inelastic scattering. *Adv. Chem. Phys.* **1977**, *36*, 141−204.
(58) Schatz, G. C. *Theory of Chemical Reaction Dynamics*; Clary, D. C., Ed.; Reidel: Dordrecht, 1986; pp 1−26.
(59) Farkas, A. Kinetik der thermischen Umwandlung von Parawasserstoff. *Z. Elektrochem. Angew. Phys. Chem.* **1930**, *36*, 782−784.
(60) Farkas, A. The thermal parahydrogen conversion. *Z. Phys. Chem. B* **1930**, *10*, 419−433.
(61) Farkas, A. *Light and Heavy Hydrogen*; Cambridge University Press, Cambridge, 1935.
(62) Farkas, A.; Farkas, L. Experiments on heavy hydrogen - V—The thermal conversion of ortho-deuterium and the interaction of hydrogen and deuterium. *Proc. R. Soc. London, Ser. A* **1935**, *152*, 124−151.
(63) Farkas, L.; Wigner, E. Calculation of the rate of elementary reactions of light and heavy hydrogen. *Trans. Faraday Soc.* **1936**, *32*, 708.
(64) London, F. Quantenmechanische Deutung des Vorgangs der Aktivierung. *Z. Electrochem. Angew. Phys. Chem.* **1929**, *35*, 552−555.
(65) Darwent, B. D.; Roberts, R. The reactions of hydrogen atoms with hydrocarbons. *Discuss. Faraday Soc.* **1953**, *14*, 55−63.
(66) Boato, G.; Careri, G.; Cimino, A.; Molinari, E.; Volpi, G. G. Homogeneous exchange reaction between hydrogen and deuterium. *J. Chem. Phys.* **1956**, *24*, 783−791.
(67) Klein, R.; McNesby, J. R.; Scheer, M. D.; Schoen, L. J. Kinetics of D atom reactions with H_2, CH_4, and D_2CO. *J. Chem. Phys.* **1959**, *30*, 58−60.
(68) Schulz, W. R.; Le Roy, D. J. Kinetics of the reaction H + *p*-H_2 = *o*-H_2 + H. *J. Chem. Phys.* **1965**, *42*, 3869−3873.
(69) Ridley, B. A.; Schulz, W. R.; Le Roy, D. J. Kinetics of the reaction D + H_2 = HD + H. *J. Chem. Phys.* **1966**, *44*, 3344−3347.
(70) Roy, D. J. L.; Ridley, B. A.; Quickert, K. A. Kinetics of the four basic thermal three-centre exchange reactions of the hydrogen isotopes. *Discuss. Faraday Soc.* **1967**, *44*, 92.
(71) Westenberg, A. A.; de Haas, N. Atom-molecule kinetics using ESR detection. II. Results for D + H_2 → HD + H and H + D_2 → HD + D. *J. Chem. Phys.* **1967**, *47*, 1393−1405.
(72) Marshall, R. M.; Purnell, J. H. The temperature-dependence of Arrhenius parameters. *J. Chem. Soc. A* **1968**, 2301−2304.
(73) Niki, T.; Mains, G. J. Chemical kinetics of the pyrolysis of hydrogen deuteride. *J. Phys. Chem. A* **1972**, *76*, 3538−3544.
(74) Mitchell, D. N.; Le Roy, D. J. Rate constants for the reaction D + H_2 = DH + H at low temperatures using ESR detection. *J. Chem. Phys.* **1973**, *58*, 3449−3453.
(75) Appel, D.; Appleton, J. P. Shock tube studies of deuterium dissociation and oxidation by atomic resonance absorption spectrophotometry. *Symp. Int. Combust. Proc.* **1975**, *15*, 701−715.
(76) Pratt, G.; Rogers, D. Homogeneous isotope exchange reactions. H_2/D_2. *J. Chem. Soc., Faraday Trans. 1* **1976**, *72*, 1589.
(77) Glass, G. P.; Chaturvedi, B. K. The rate of the reaction D + $H_2(v = 1)$ → DH + H. *J. Chem. Phys.* **1982**, *77*, 3478−3484.
(78) Rozenshtein, V. B.; Gershenzon, Y. M.; Ivanov, A. V.; Il'in, S. D.; Kucheryavii, S. I.; Umanskii, S. Y. The temperature dependence of the reactions $H_2(v = 1)$ + D, H. *Chem. Phys. Lett.* **1985**, *121*, 89−93.
(79) Dreier, T.; Wolfrum, J. Experimental study of the D + H_2 (v = 1) reaction by CARS spectroscopy. *Int. J. Chem. Kinet.* **1986**, *18*, 919−935.
(80) Miyazaki, T.; Lee, K. P. Direct evidence for the tunneling reaction of HD + D → H + D_2 in the radiolysis of a D_2−HD mixture at 4.2 K. *J. Phys. Chem. A* **1986**, *90*, 400−402.
(81) Reid, I. D.; Garner, D. M.; Lee, L. Y.; Senba, M.; Arseneau, D. J.; Fleming, D. G. Experimental tests of reaction rate theory: Mu + H_2 and Mu + D_2. *J. Chem. Phys.* **1987**, *86*, 5578−5583.
(82) Michael, J. V.; Fisher, J. R. Rate constants for the reaction D + H_2 → HD + H, over the temperature range 655−1979 K, by the flash photolysis−shock tube technique. *J. Phys. Chem. A* **1990**, *94*, 3318−3323.
(83) Michael, J. V.; Fisher, J. R.; Bowman, J. M.; Sun, Q. Theoretical and experimental rate constants for two isotopic modifications of the reaction H + H_2. *Science* **1990**, *249*, 269−271.
(84) Michael, J. V.; Su, M.-C.; Sutherland, J. W. New rate constants for D + H_2 and H + D_2 between ∼ 1150 and 2100 K. *J. Phys. Chem. A* **2004**, *108*, 432−437.
(85) Shavitt, I. A calculation of the rates of the ortho-para conversions and isotope exchanges in hydrogen. *J. Chem. Phys.* **1959**, *31*, 1359−1367.
(86) Weston, R. E. H_3 activated complex and the rate of reaction of hydrogen atoms with hydrogen molecules. *J. Chem. Phys.* **1959**, *31*, 892−898.
(87) Garrett, B. C.; Truhlar, D. G. Generalized transition state theory calculations for the reactions D + H_2 and H + D_2 using an accurate potential energy surface: Explanation of the kinetic isotope effect. *J. Chem. Phys.* **1980**, *72*, 3460−3471.

https://doi.org/10.1021/acs.jpca.6c01349
J. Phys. Chem. A 2026, 130, 6312−6326

(88) Blais, N. C.; Truhlar, D. G. Product state distributions for inelastic and reactive H + D_2 collisions as functions of collision energy. *J. Chem. Phys.* **1985**, *83*, 2201−2206.
(89) Garrett, B. C.; Truhlar, D. G.; Schatz, G. C. Test of variational transition state theory and multidimensional semiclassical transmission coefficients methods against accurate quantal rate constants for H + H_2/HD, D + H_2, and O + H_2/D_2/HD, including intra- and intermolecular kinetic isotope effects. *J. Am. Chem. Soc.* **1986**, *108*, 2876−2881.
(90) Webster, F.; Light, J. C. Reactive scattering of H + H_2 and its isotopic analogs. *J. Chem. Phys.* **1986**, *85*, 4744−4745.
(91) Pack, R. T.; Parker, G. A. Quantum reactive scattering in three dimensions using hyperspherical (APH) coordinates. Theory. *J. Chem. Phys.* **1987**, *87*, 3888−3921.
(92) Schwenke, D. W.; Haug, K.; Truhlar, D. G.; Sun, Y.; Zhang, J. Z. H.; Kouri, D. J. Variational basis-set calculations of accurate quantum mechanical reaction probabilities. *J. Phys. Chem. A* **1987**, *91*, 6080−6082.
(93) Takayanagi, T.; Masaki, N.; Nakamura, K.; Okamoto, M.; Sato, S.; Schatz, G. C. The rate constants for the H + H_2 reaction and its isotopic analogs at low temperatures: Wigner threshold law behavior. *J. Chem. Phys.* **1987**, *86*, 6133−6139.
(94) Zhang, J. Z.; Miller, W. H. New method for quantum reactive scattering, with applications to the 3-D H + H_2 reaction. *Chem. Phys. Lett.* **1987**, *140*, 329−337.
(95) Schatz, G. C. Quantum effects in gas phase bimolecular chemical reactions. *Annu. Rev. Phys. Chem.* **1988**, *39*, 317−340.
(96) Park, T. J.; Light, J. C. Quantum thermal rate constants for the exchange reactions of hydrogen isotopes: D + H_2. *J. Chem. Phys.* **1991**, *94*, 2946−2955.
(97) Mielke, S. L.; Lynch, G. C.; Truhlar, D. G.; Schwenke, D. W. Ab initio chemical kinetics: Converged quantal reaction rate constants for the D + H_2 system. *J. Phys. Chem. A* **1994**, *98*, 8000−8008.
(98) Aoiz, F. J.; Bañares, L.; Díez-Rojo, T.; Herrero, V. J.; Sáez Rábanos, V. Reaction cross section and rate constant calculations for the D + $H_2(v = 0,1)$ → HD + H reaction on three ab initio potential energy surfaces. A quasiclassical trajectory study. *J. Phys. Chem. A* **1996**, *100*, 4071−4083.
(99) Bañares, L.; D'Mello, M. Quantum mechanical rate constants for the D + H_2 → HD + H reaction on the BKMP2 potential energy surface. *Chem. Phys. Lett.* **1997**, *277*, 465−472.
(100) Kendrick, B. K. Quantum reactive scattering calculations for the H + D_2 → HD + D reaction. *J. Chem. Phys.* **2001**, *114*, 8796−8819.
(101) Sukiasyan, S.; Meyer, H.-D. Reaction cross sections for the H + $D_2(v = 1)$ → HD + D and D + $H_2(v = 1)$ → DH + H systems. A multiconfiguration time-dependent Hartree (MCTDH) wave packet propagation study. *J. Chem. Phys.* **2002**, *116*, 10641−10647.
(102) Kendrick, B. K. Quantum reactive scattering calculations for the D + H_2 → HD + H reaction. *J. Chem. Phys.* **2003**, *118*, 10502−10522.
(103) Aoiz, F. J.; Banares, L.; Herrero, V. J. The H + H_2 reactive system. Progress in the study of the dynamics of the simplest reaction. *Int. Rev. Phys. Chem.* **2005**, *24*, 119−190.
(104) Xie, Y.; Zhao, H.; Wang, Y.; Huang, Y.; Wang, T.; Xu, X.; Xiao, C.; Sun, Z.; Zhang, D. H.; Yang, X. Quantum interference in H + HD → H_2+ D between direct abstraction and roaming insertion pathways. *Science* **2020**, *368*, 767−771.
(105) Wang, Y.; Huang, J.; Wang, W.; Du, T.; Xie, Y.; Ma, Y.; Xiao, C.; Zhang, Z.; Zhang, D. H.; Yang, X. Stereodynamical control of the H + HD → H_2 + D reaction through HD reagent alignment. *Science* **2023**, *379*, 191−195.
(106) Li, S.; Huang, J.; Lu, Z.; Shu, Y.; Chen, W.; Yuan, D.; Wang, T.; Fu, B.; Zhang, Z.; Wang, X.; Zhang, D. H.; Yang, X. Observation of geometric phase effect through backward angular oscillations in the H + HD → H_2 + D reaction. *Nat. Commun.* **2024**, *15*, 1698.
(107) Fang, Y.; Huang, J.; Zhang, D. H. Ultracold D + H_2 (v = 4, j = 0) reaction dynamics: Long-range interactions, diagonal Born−Oppenheimer correction, and a diabatic geometric phase treatment. *J. Chem. Phys.* **2026**, *164*, 024302.
(108) Liu, B. Ab initio potential energy surface for linear H_3. *J. Chem. Phys.* **1973**, *58*, 1925−1937.
(109) Siegbahn, P.; Liu, B. An accurate three-dimensional potential energy surface for H_3. *J. Chem. Phys.* **1978**, *68*, 2457−2465.
(110) Truhlar, D. G.; Horowitz, C. J. Functional representation of Liu and Siegbahn's accurate *ab initio* potential energy calculations for H + H_2. *J. Chem. Phys.* **1978**, *68*, 2466−2476.
(111) Truhlar, D. G.; Horowitz, C. J. Erratum: Functional representation of Liu and Siegbahn's accurate ab initio potential energy calculations for H + H_2. *J. Chem. Phys.* **1979**, *71*, 1514.
(112) Varandas, A. J. C. A LEPS potential for H_3 from force field data. *J. Chem. Phys.* **1979**, *70*, 3786−3795.
(113) Varandas, A. J. C.; Brown, F. B.; Mead, C. A.; Truhlar, D. G.; Blais, N. C. A double many-body expansion of the two lowest-energy potential surfaces and nonadiabatic coupling for H_3. *J. Chem. Phys.* **1987**, *86*, 6258−6269.
(114) Boothroyd, A. I.; Keogh, W. J.; Martin, P. G.; Peterson, M. R. An improved H_3 potential energy surface. *J. Chem. Phys.* **1991**, *95*, 4343−4359.
(115) Boothroyd, A. I.; Keogh, W. J.; Martin, P. G.; Peterson, M. R. A refined H_3 potential energy surface. *J. Chem. Phys.* **1996**, *104*, 7139−7152.
(116) Mark Wu, Y.-S.; Kuppermann, A.; Anderson, J. B. A very high accuracy potential energy surface for H_3. *Phys. Chem. Chem. Phys.* **1999**, *1*, 929−937.
(117) Mielke, S. L.; Garrett, B. C.; Peterson, K. A. A hierarchical family of global analytic Born−Oppenheimer potential energy surfaces for the H + H_2 reaction ranging in quality from double-zeta to the complete basis set limit. *J. Chem. Phys.* **2002**, *116*, 4142−4161.
(118) Ghosh, A.; Roy, A.; Kumar, A.; Naskar, K.; Ravi, S.; Adhikari, S. Beyond Born−Oppenheimer constructed diabatic potential energy surfaces for H_3: Adiabatic and diabatic reaction probabilities. *J. Phys. Chem. A* **2025**, *129*, 6315−6332.
(119) Born, M.; Oppenheimer, J. R. Zur Quantentheorie der Molekeln. *Ann. Phys.* **1927**, *389*, 457−484.
(120) Handy, N. C.; Yamaguchi, Y.; Schaefer, H. F., III The diagonal correction to the Born−Oppenheimer approximation: its effect on the singlet-triplet splitting of CH_2 and other molecular effects. *J. Chem. Phys.* **1986**, *84*, 4481−4484.
(121) Valeev, E. F.; Sherrill, C. D. The diagonal Born−Oppenheimer correction beyond the Hartree−Fock approximation. *J. Chem. Phys.* **2003**, *118*, 3921−3927.
(122) Garrett, B. C.; Truhlar, D. G.; Grev, R. S.; Walker, R. B. Comparison of variational transition state theory and the unified statistical model with vibrationally adiabatic transmission coefficients to accurate collinear rate constants for T + HD → TH + D. *J. Chem. Phys.* **1980**, *73*, 235−240.
(123) Walker, R. B.; Hayes, E. F. Theoretical analysis of the quantum contributions to the reactions H_2 (v = 1) + H → H + H(v = 0, 1) and H_2 (v = 1) + D → H + HD(v'=0,1). *J. Phys. Chem. A* **1983**, *87*, 1255−1263.
(124) Zhang, J. Z.; Miller, W. H. Quantum reactive scattering via the S-matrix version of the Kohn variational principle: Integral cross sections for H + $H_2(v_1=j_1=0)$ → $H_2(v_2=1,j_2=1,3)$ + H in the energy range E_{total} = 0.9−1.4 eV. *Chem. Phys. Lett.* **1988**, *153*, 465−470.
(125) Blais, N. C.; Zhao, M.; Mladenovic, M.; Truhlar, D. G.; Schwenke, D. W.; Sun, Y.; Kouri, D. J. Comparison of quasiclassical trajectory calculations to accurate quantum mechanics for state-to-state partial cross sections at low total angular momentum for the reaction D + H_2 → HD + H. *J. Chem. Phys.* **1989**, *91*, 1038−1042.
(126) Wang, D.; Bowman, J. M. New reduced dimensionality calculations of cumulative reaction probabilities and rate constants for the H + H_2 and D + H_2 reactions. *J. Phys. Chem. A* **1994**, *98*, 7994−7999.
(127) Bañares, L.; Aoiz, F. J.; Herrero, V. J.; D'Mello, M. J.; Niederjohann, B.; Seekamp-Rahn, K.; Wrede, E.; Schnieder, L.

Experimental and quantum mechanical study of the H+D_2 reaction near 0.5 eV: The assessment of the H_3 potential energy surfaces. *J. Chem. Phys.* **1998**, *108*, 6160−6169.
(128) Aoiz, F. J.; Bañares, L.; Castillo, J. F. On the existence of resonances in the H + D_2 → HD(v'=0, j'=7) + D reaction at collision energies 0.6−1.3 eV. *J. Chem. Phys.* **2001**, *114*, 8237−8239.
(129) Mielke, S. L.; Peterson, K. A.; Schwenke, D. W.; Garrett, B. C.; Truhlar, D. G.; Michael, J. V.; Su, M.-C.; Sutherland, J. W. H + H_2 thermal reaction: A convergence of theory and experiment. *Phys. Rev. Lett.* **2003**, *91*, 063201.
(130) Suleimanov, Y. V.; De Tudela, R. P.; Jambrina, P. G.; Castillo, J. F.; Sáez-Rábanos, V.; Manolopoulos, D. E.; Aoiz, F. J. A ring polymer molecular dynamics study of the isotopologues of the H + H_2 reaction. *Phys. Chem. Chem. Phys.* **2013**, *15*, 3655.
(131) Ranga, S.; Ghosal, S. Accurate quantum mechanical rate coefficients for D+H_2(v, j) reaction: From ultracold to thermal temperature limit. *Comput. Theor. Chem.* **2017**, *1102*, 69−73.
(132) Rozenshtein, V.; Gershenzon, Y.; Ivanov, A.; Kucheryavii, S. Experimental study of the D + H_2 (v = 1) reaction. *Chem. Phys. Lett.* **1984**, *105*, 423−426.
(133) Park, T. J.; Light, J. C. Quantum flux operators and thermal rate constant: Collinear H + H_2. *J. Chem. Phys.* **1988**, *88*, 4897−4912.
(134) Thompson, W. H.; Miller, W. H. On the "direct" calculation of thermal rate constants. II. The flux-flux autocorrelation function with absorbing potentials, with application to the O + HCl → OH + Cl reaction. *J. Chem. Phys.* **1997**, *106*, 142−150.
(135) Schlag, E. W. Symmetry numbers and reaction rates. *J. Chem. Phys.* **1963**, *38*, 2480−2482.
(136) Quack, M. Detailed symmetry selection rules for reactive collisions. *Mol. Phys.* **1977**, *34*, 477−504.
(137) Császár, A. G.; Fábri, C.; Szidarovszky, T.; Mátyus, E.; Furtenbacher, T.; Czakó, G. The fourth age of quantum chemistry: molecules in motion. *Phys. Chem. Chem. Phys.* **2012**, *14*, 1085−1106.
(138) Fábri, C.; Mátyus, E.; Császár, A. G. Numerically constructed internal-coordinate Hamiltonian with Eckart embedding and its application for the inversion tunneling of ammonia. *Spectrochim. Acta, Part A* **2014**, *119*, 84−89.
(139) Fábri, C.; Quack, M.; Császár, A. G. On the use of nonrigid-molecular symmetry in nuclear-motion computations employing a discrete variable representation: a case study of the bending energy levels of CH_5^+. *J. Chem. Phys.* **2017**, *147*, 134101.
(140) Papp, D.; Szidarovszky, T.; Császár, A. G. A general variational approach for computing rovibrational resonances of polyatomic molecules. Application to the weakly bound H_2He^+ and H_2·CO systems. *J. Chem. Phys.* **2017**, *147*, 094106.
(141) Simkó, I.; Szidarovszky, T.; Császár, A. G. Toward automated variational computation of rovibrational resonances, including a case study of the H_2 dimer. *J. Chem. Theory Comput.* **2019**, *15*, 4156−4169.
(142) Simkó, I.; Fábri, C.; Császár, A. G. Quantum-Chemical and Quantum-Graph Models of the Dynamical Structure of CH_5^+. *J. Chem. Theory Comput.* **2023**, *19*, 42−50.
(143) Simkó, I.; Schran, C.; Brieuc, F.; Fábri, C.; Asvany, O.; Schlemmer, S.; Marx, D.; Császár, A. G. Quantum nuclear delocalization and its rovibrational fingerprints. *Angew. Chem., Int. Ed.* **2023**, *62*, e202306744.
(144) Light, J. C.; Carrington, T. Discrete variable representations and their utilization. *Adv. Chem. Phys.* **2000**, *114*, 263−310.
(145) Lanczos, C. An iteration method for the solution of the eigenvalue problem of linear differential and integral operators. *J. Res. Natl. Bur. Stand.* **1950**, *45*, 255−282.
(146) Cullum, J. K.; Willoughby, R. A. *Lanczos Algorithm for Large Symmetric Eigenvalue Computations*; Birkhäuser, Boston, 1985.
(147) Manthe, U. Reaction rates: Accurate quantum dynamical calculations for polyatomic systems. *J. Theor. Comput. Chem.* **2002**, *01*, 153−172.
(148) Tal-Ezer, H.; Kosloff, R. An accurate and efficient scheme for propagating the time dependent Schrödinger equation. *J. Chem. Phys.* **1984**, *81*, 3967−3971.
(149) Leforestier, C.; Bisseling, R. H.; Cerjan, C.; Feit, M. D.; Friesner, R.; Guldberg, A.; Hammerich, A.; Jolicard, G.; Karrlein, W.; Meyer, H.-D.; Lipkin, N.; Roncero, O.; Kosloff, R. A comparison of different propagation schemes for the time dependent Schrödinger equation. *J. Comput. Phys.* **1991**, *94*, 59−80.
(150) Kosloff, R. Propagation methods for quantum molecular dynamics. *Annu. Rev. Phys. Chem.* **1994**, *45*, 145−178.
(151) Lehoucq, R. B.; Sorensen, D. C.; Yang, C. *ARPACK: Solution of Large Scale Eigenvalue Problems by Implicitly Restarted Arnoldi Methods*. **1997**.
(152) Jacobi, C. G. J. Sur l'élimination des noeuds dans le probléme des trois corps. *Astron. Nachr.* **1843**, *15*, 236−255.
(153) Colbert, D. T.; Miller, W. H. A novel discrete variable representation for quantum mechanical reactive scattering via the S-matrix Kohn method. *J. Chem. Phys.* **1992**, *96*, 1982−1991.
(154) Moiseyev, N. *Non-Hermitian Quantum Mechanics*; Cambridge University Press, Cambridge, 2011.
(155) Gamache, R. R.; Roller, C.; Lopes, E.; Gordon, I. E.; Rothman, L. S.; Polyansky, O. L.; Zobov, N. F.; Kyuberis, A. A.; Tennyson, J.; Yurchenko, S. N.; Császár, A. G.; Furtenbacher, T.; Huang, X.; Schwenke, D. W.; Lee, T. J.; Drouin, B. J.; Tashkun, S. A.; Perevalov, V. I.; Kochanov, R. V. Total internal partition sums for 166 isotopologues of 51 molecules important in planetary atmospheres: Application to HITRAN 2016 and beyond. *J. Quant. Spectrosc. Radiat. Transfer* **2017**, *203*, 70−87.
(156) Turányi, T.; Zsély, I. G.; Papp, M.; Nagy, T.; Furtenbacher, T.; Tóbiás, R.; Árendás, P.; Császár, A. G. ReSpecTh: Reaction kinetics, spectroscopy, and thermochemical datasets. *Sci. Data* **2025**, *12*, 1021.
(157) Popovas, A.; Jørgensen, U. G. Partition functions: I. Improved partition functions and thermodynamic quantities for normal, equilibrium, and ortho and para molecular hydrogen. *Astron. Astrophys.* **2016**, *595*, A130.
(158) Wu, Y.-S. M.; Kuppermann, A. Prediction of the effect of the geometric phase on product rotational state distributions and integral cross sections. *Chem. Phys. Lett.* **1993**, *201*, 178−186.
(159) Kendrick, B. K. Geometric Phase Effects in Chemical Reaction Dynamics and Molecular Spectra. *J. Phys. Chem. A* **2003**, *107*, 6739−6756.
(160) Carlos Juanes-Marcos, J.; Althorpe, S. C. On the role of the conical intersection in H+H_2 reactive scattering. *Chem. Phys. Lett.* **2003**, *381*, 743−750.
(161) Aharonov, Y.; Bohm, D. Significance of electromagnetic potentials in the quantum theory. *Phys. Rev.* **1959**, *115*, 485−491.
(162) Fábri, C.; Marquardt, R.; Császár, A. G.; Quack, M. Controlling tunneling in ammonia isotopomers. *J. Chem. Phys.* **2019**, *150*, 014102.

https://doi.org/10.1021/acs.jpca.6c01349
J. Phys. Chem. A 2026, 130, 6312−6326